Journal of the American Chemical Society (JACS) *142* (2020): 21017–21031

**DOI:** https://doi.org/10.1021/jacs.0c07291

# Dual-Mode Chiral Self-Assembly of Cone-shaped Subphthalocyanine Aromatics

María J. Mayoral,[†] Julia Guilleme,[†] Joaquín Calbo,[‡] Juan Aragó,[‡] Fátima Aparicio,[†] Enrique Ortí,*[,‡] Tomás Torres,*[,†,#,§] and David González-Rodríguez*[,†,#]

[†] Departamento de Química Orgánica, Universidad Autónoma de Madrid, 28049 Madrid, Spain

[‡] Instituto de Ciencia Molecular, Universidad de Valencia, 46980 Paterna (Valencia), Spain

[#] Institute for Advanced Research in Chemical Sciences (IAdChem), Universidad Autónoma de Madrid, 28049 Madrid Spain

[§] IMDEA Nanociencia, c/ Faraday 9, Campus de Cantoblanco, 28049 Madrid, Spain

*KEYWORDS: Self-assembly, Subphthalocyanine, Supramolecular Polymers, Porphyrinoids*

**ABSTRACT:** Columnar polymers and liquid crystals obtained from π-conjugated cone-shaped molecules are rising increasing interest due to the possibility of obtaining unconventional polar organizations that show anisotropic charge transport and unique chiroptical properties. However, and in contrast to the more common planar discotics, the self-assembly of conic or pyramidic molecules in solution remains largely unexplored. Here, we show how a molecular geometry change, from flat to conic, can generate supramolecular landscapes where different self-assembled species, each of them being under thermodynamic equilibrium with the monomer, exist exclusively within distinct regimes. In particular, depending on the solvent nature – aromatic or aliphatic – cone-shaped $C_3$-symmetric subphthalocyanine **1** can undergo self-assembly either as a tail-to-tail dimer, showing monomer-dimer sigmoidal transitions, or as a head-to-tail non-centrosymmetric columnar polymer, exhibiting a nucleation-elongation polymerization mechanism. Moreover, the experimental and theoretical comparison between racemic and enantiopure samples revealed that the two enantiomers (**1*M*** and **1*P***) tend to narcissistically self-sort in the dimer regime, each enantiomer showing a strong preference to associate with itself, but socially self-sort in the polymer regime, favoring an alternate stacking order along the columns.

## INTRODUCTION

π-Conjugated discotics are a well-known, attractive class of molecules with great potential in organic liquid crystal and optoelectronic technologies.[1,2] This is due to their strong tendency to order in columnar architectures, driven by the stacking of their extended planar cores, which results in efficient intermolecular π-π overlaps and is the origin of bulk semiconducting properties. Perylenes, acenes, phthalocyanines, porphyrins, triphenylenes, and hexabenzocoronenes are just a few examples of relevant flat molecules that have been the subject of myriads of studies focused on their properties and columnar organization, not only in condensed phases,[3] but also in solution.[4]

Now, when molecular structure deviates from planarity, as in cone-shaped molecules – also named conic, bowlic, or pyramidic –,[5] additional intriguing properties may arise as a consequence of their stacking. First, a molecule with a conic shape or cone conformations[6] may present axial dipoles that can interact with electric fields and, if piled up in columns and aligned uniaxially, give rise to polarly ordered materials[7] exhibiting switchable (*i.e.*, ferroelectric)[8,9] or permanent[10,11] polarization, as well as anisotropic charge transport.[9b,12] As a matter of fact, conic molecules are contributing strongly to the renovated interest in the field of supramolecular ferroelectrics and polar assemblies, where novel materials with unprecedented physical properties are being developed from molecular design.[13] A second important difference with respect to planar discotics is that, when properly substituted, a pyramidal molecule may become chiral[14] and will thus have the possibility of forming homochiral helical assemblies.[15,16] As opposed to the many examples of helically stacked discotics where chiral centers are placed in the disordered peripheral chains,[17] chirality resides here intrinsically in the aromatic core of the molecule. Finally, contrarily to flat discotics, a cone-shaped molecule may show diverse aggregation modes (Figure 1). Since they display a convex side (a head) and a concave side (a tail), intermolecular stacking interactions between two pyramidal molecules may in principle lead to three distinct geometries: centrosymmetric *head-to-head* and *tail-to-tail* interactions, and a non-centrosymmetric *head-to-tail* aggregation mode. Only the latter can produce polymeric columns with a polar organization.

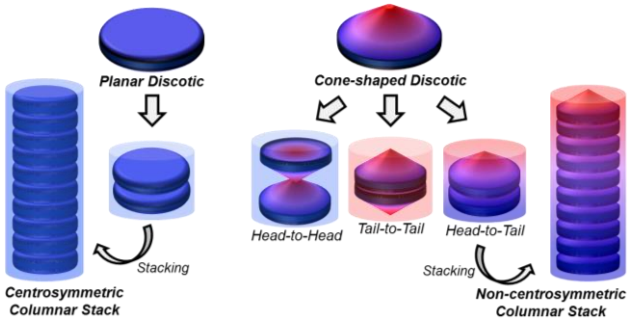


**Figure 1.** Potential stacking modes for planar discotics and pyramidic molecules.

However, many of the available cone- or bowl-shaped π-conjugated molecules that can potentially generate these remarkable properties, such as sumanene, coronene, calixarene, cyclotriveratrylene, etc., exhibit relatively fast bowl inversion that eventually results in dipole cancellations and, in the case of chiral molecules, in racemization.[18] Subphthalocyanines (SubPcs),[19] on the other hand, are an important class of $C_3$-symmetric organic semiconductors with a singular rigid pyramidal structure in which cone inversion is blocked due to tetrahedral coordination of a central boron atom to three isoindoles and to an axial ligand.[20] As a consequence, these unique molecules are endowed with permanent axial dipoles and their enantiomers show no racemization.[14a,16] Unfortunately, most axial ligands used in SubPcs are too bulky and efficiently prevent aggregation, which has been so far the basis of many of the applications of these highly soluble magenta dyes in the fields of nonlinear

optics,[21] photodynamic therapy,[22] artificial photosynthetic mimics,[23] or organic optoelectronics.[24]

Nonetheless, we demonstrated that SubPc head-to-tail columnar stacking can be promoted by providing these molecules with a very small axial ligand: a fluorine atom.[16,25] Moreover, the presence of a strongly polar axial B-F bond additionally reinforces head-to-tail association due to dipole-dipole interactions and lead to unprecedented columnar liquid-crystalline materials that can be oriented in the presence of electric fields and that exhibit permanent[10] or switchable[9b] polarization. We also showed that these non-centrosymmetric columnar assemblies can be stabilized in alkane media by equipping the SubPcBF core with arylamide substitutents (as in **1**; Figure 2a),[16] which originated the first lyotropic columnar nematic mesophases exhibiting polar switching.[9a]

Here, we investigate in detail the solution self-assembly of SubPc **1** and demonstrate how a geometry change from the common flat discotic to the unusual cone-shaped pyramidic can generate a more complex supramolecular landscape where different self-assembled species, each of them being under thermodynamic equilibrium with the monomer, exist exclusively within distinct regimes. Specifically, depending solely on the solvent nature – aromatic or aliphatic –,[26] π-conjugated SubPc **1** can self-assemble either in a tail-to-tail dimer, showing monomer-dimer sigmoidal transitions (*Regime A*), or in a head-to-tail columnar stack, formed *via* a nucleation-growth polymerization mechanism (*Regime B*). Furthermore, if the two enantiomers of this $C_3$-symmetric molecule (**1*P*** and **1*M***; Figure 2a)[19a] are separated by chiral HPLC,[16] homochiral assemblies can be then produced that show opposite helicities. Additional spectroscopic and computational studies, comparing the assembly of racemic and enantiopure **1** samples, demonstrate that each of these aggregation modes additionally reveals prominent and exclusive chiral self-sorting behavior. Whereas the SubPc enantiomers socially self-sort in the polymer regime (*Regime B*), showing an alternate columnar stacking order, they reveal narcissistic self-sorting in the dimer regime (*Regime A*), each enantiomer disclosing a strong preference to associate with itself. Our studies also provide a deeper insight into some unique structural features of both self-assembled species, especially regarding the conformational arrangement of the exocyclic dipolar H-bonded amide groups.

## RESULTS AND DISCUSSION

**Tail-to-Tail Dimer *vs* Head-to-Tail Polymer Aggregation Regimes.** $C_3$-symmetric SubPc **1** exhibits quite distinct absorption, emission, and circular dichroism (CD) features as a function of the solvent environment. Figures 2b-c display the spectra of **1** in the three main solvents employed in this work: 1,4-dioxane, toluene, and methylcyclohexane (MCH). The corresponding spectra in the same conditions of **2**, featuring a bulky *tert*-butylphenoxy axial ligand instead of the fluorine atom, are shown as well for comparison

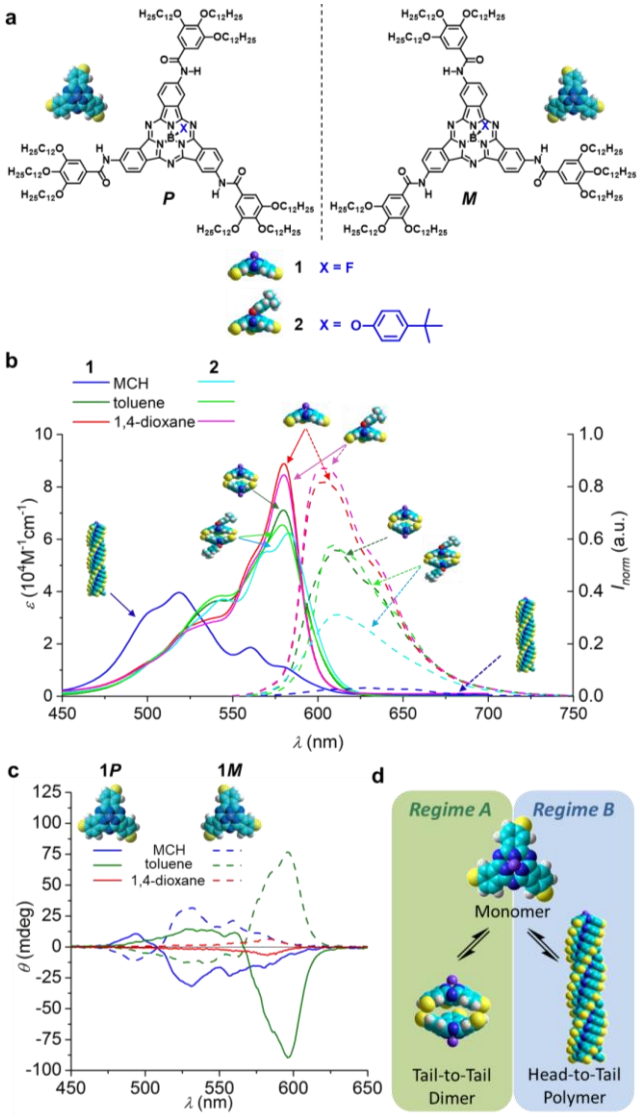


**Figure 2**. (a) Structure of SubPcs **1** and **2**. (b) Absorption (solid lines) and emission (dashed lines; $\lambda_{exc}$ = 530 nm) spectra of **1** and **2** in dioxane, toluene, and MCH. Emission spectra were recorded for the same samples of the displayed absorption spectra exciting at 530 nm, where all samples show virtually identical absorbance. (c) CD spectra of **1*P*** and **1*M*** in dioxane, toluene, and MCH. In all cases: [**1**] = [**2**] = $3.2 \times 10^{-5}$ M; T = 20 °C. (d) Model of the different self-assembly regimes studied in this work. Yellow spheres in the model represent the arylamide substituents.

**1** and **2** solutions in 1,4-dioxane (red and pink spectra in Figure 2b) show the typical narrow *Q*-band absorption characteristics of monomeric SubPcs with a maximum at 580 nm (***ε*** = 88.900 (**1**) and 84600 $M^{-1}$ $cm^{-1}$ (**2**)) and shoulders at 560 and 530 nm. Steady-state fluorescence experiments revealed strong emission bands for both compounds with a maximum at 603 nm. On the other hand, the two enantiomers of **1** (**1*P*** and **1*M***)[16] in this solvent exhibit weak mirror-image CD signals with low-intensity maxima at 583 nm, negative for the former and positive for the latter (Figure 2c). In toluene, on the contrary, both **1** and **2** show clear signs of (partial) aggregation (green spectra in Figures 2b,c). The *Q*-band is slightly broadened and a new absorption shoulder arises at 542 nm, while fluorescence emission is slightly quenched and red-shifted for both compounds in comparison to dioxane. The CD spectrum of **1*P*** shows now a

pronounced negative maximum at 596 nm and zero-crossing at 567 nm. The enantiomer **1*M*** shows obviously mirror-image signals. The situation changes again in MCH, where the spectral features of **1** or **2** are now totally different (blue spectra in Figures 2b,c). **1** solutions in MCH display a broad, blue-shifted *Q*-band with maxima at 518 nm ($\varepsilon$ = 39600 $M^{-1}$ $cm^{-1}$) and a shoulder at 501 nm, while the emission is now almost fully quenched (by a factor of 25) with respect to the monomer in dioxane. The CD spectrum shows maxima at 494 nm (+), 531 nm (–), and 557 nm (–) for **1*P***, whereas **1*M*** displays a mirror-image spectrum with opposite signs. On the other hand, the spectral characteristics in MCH of **2**, equipped with the bulky axial ligand, are reminiscent of those found in toluene, suggesting that the same supramolecular species is formed in both solvents.

From these observations we propose that each solvent media promotes a different regime, and thus the prevalence of one particular supramolecular species (Figure 2d). In dioxane (and also tetrahydrofurane (THF)), a competing solvent for H-bonding, both compounds are fully dissociated, and the monomer is the dominant species in solution. In these solvents, the absorption features of **1** or **2** are identical independently of sample concentration and temperature and the $^1$H NMR spectra showed sharp signals characteristic of monomeric SubPcs (see below).

On the contrary, in MCH (and also heptane or dodecane), a strongly nonpolar aliphatic solvent, **1** aggregates head-to-tail to form polymeric columnar π–π stacks, as observed in AFM and TEM microscopy measurements (see Figures S1A-C). Width dimensions obtained by TEM, between 4.5 and 6 nm, matched rather well the outer diameter expected for the columnar stacks of SubPc **1**. AFM height profiles showed however smaller diameters, between 2 and 3 nm, rather matching the rigid aromatic SubPc core (see Figure S1C), which is usually due to the compression of side-chains by the force applied by the AFM probe, and by the affinity of the assemblies for the surface. As noticed in our previous work, the formation of these fibers can ultimately lead to solvent gelation and to lyotropic mesophases if the concentration is high enough.[9a] However, due to obvious steric hindrance caused by the bulky axial substituent, **2** cannot polymerize in head-to-tail stacks. The best option for this molecule to satisfy the involvement of the amide groups in H-bonding is to dimerize by tail-to-tail interactions. Compared to the shape-complementary concave-convex association, the π-conjugated cores show only a moderate overlap in this concave-concave association mode, which is principally characterized by a slightly broadened absorption *Q*-band and an intense CD signal at 596 nm. It should be noted that a related molecule in which the amide units are replaced by ethynylene groups[10] shows no association in solution, even at the highest concentrations measured in MCH or dodecane, which suggests that the main driving force for SubPc **1**/**2** association is H-bonding between arylamide groups.

Finally, in toluene (and also chlorobenzene or 1-phenyloctane), a nonpolar solvent but a good solvating agent for π-surfaces, these last spectral features are retained for both compounds, so we assume that the formation of tail-to-tail H-bonded dimers is predominant for both **1** and **2**.

To further prove these assumptions, we conducted optical experiments as a function of the three main parameters that rule self-assembly: temperature, concentration, and environment (*i.e.*, solvent nature). Due to the clear changes observed and its sensitivity, UV-vis absorption was considered the most appropriate technique to monitor the association transitions between supramolecular species and fit the data to suitable models, as described below. The supramolecular transitions of racemic **1** and **2** were compared in the same conditions and monitored at $\lambda$ = 580 nm. Our results are displayed in the set of experiments described below, where the three species can be readily distinguished based on their extinction coefficients at 580 nm: monomer ($\varepsilon_{580}$ ~ 88.000 $M^{-1}$ $cm^{-1}$), dimer ($\varepsilon_{580}$ ~ 60.000 $M^{-1}$ $cm^{-1}$), and polymer ($\varepsilon_{580}$ ~ 12.000 $M^{-1}$ $cm^{-1}$). These coefficients do not depend strongly on solvent composition or the nature of the axial ligand. In all cases, the degree of aggregation ($\alpha_{agg}$) lowers with increasing temperature and decreasing concentration in both toluene and MCH, while cooling and heating curves overlap each other, which is consistent with supramolecular aggregation under thermodynamic control.

*Temperature-dependent measurements.* Figures 3a and 3b show the absorption changes recorded for the dissociation of the **1** tail-to-tail dimer in toluene and the **1** head-to-tail polymer in MCH, respectively, as a function of temperature (from –5 to 95 ºC). In Figures 3c and 3d we plot the corresponding extinction coefficient changes observed at 580 nm for **1** and **2** in toluene and MCH, respectively, at different concentrations. The corresponding set of spectra are collected in Figure S2 in the S.I. The variable-temperature fluorescence emission spectra, shown in Figure S3, closely match the trends recorded from UV-vis absorption measurements.

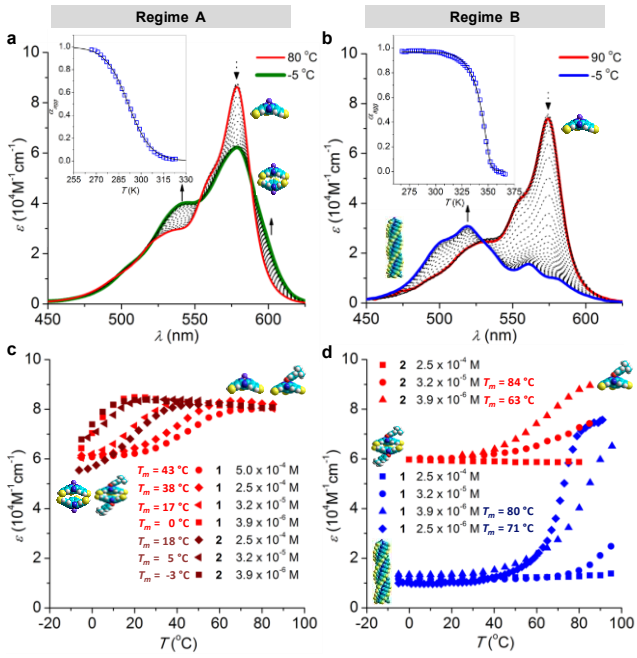


**Figure 3**. (a,b) **1** *Q*-band absorption changes as a function of temperature in (a) toluene at 2.5 × $10^{-4}$ M and (b) MCH at 2.5 × $10^{-6}$ M (scan rate: 0.5 K $min^{-1}$, to ensure that the process takes place under thermodynamic control). Arrows indicate spectral changes upon temperature decrease. Insets: relationship between the degree of aggregation and temperature and the corresponding fit (solid line) to isodesmic (a) and nucleation-elongation (b) models. (c,d) Molar absorption changes monitored at 580 nm in toluene (c) and MCH (d) of **1** or **2** solutions at different concentrations. In red: *Regime A*. In blue: *Regime B*. $T_m$ is the melting temperature (temperature at which $\alpha$ = 0.5) calculated in each experiment. The corresponding set of spectra can be found in the S.I. (Figure S2).

**Table 1. Thermodynamic Parameters Calculated upon (a) Polymerization by Decreasing Temperature in MCH, and (b) Depolymerization in MCH:Dioxane mixtures by Increasing the Volume Fraction of Dioxane ($\chi_D$).**

| | | $K_n$ ($M^{-1}$)[a] | $K_e$ ($M^{-1}$)[b] | $T_e$ (K)[c] | $\sigma$ [d/j] | $\Delta H^0$ (kJ mol$^{-1}$)[e] | $\Delta S^0$ (J mol$^{-1}\cdot$K$^{-1}$)[f] | $\Delta H_n^0$ (kJ mol$^{-1}$)[g] | $m$ (kJ mol$^{-1}$)[h] | $\Delta G^0$ (kJ mol$^{-1}$)[i] |
|---|---|---|---|---|---|---|---|---|---|---|
| a | **1** | $1.5 \times 10^3$ | $3.7 \times 10^5$ | 350.3 ± 0.3 | 0.004 | –97.4 ± 2.7 | –17.1 ± 0.8 | –16.3 ± 1.1 | - | - |
| | **1*M*** | $7.1 \times 10^3$ | $4.2 \times 10^5$ | 344.9 ± 1.1 | 0.017 | –56.1 ± 3.4 | –55.0 ± 2.8 | –11.7 ± 1.3 | - | - |
| b | **1** | - | - | | 0.027 | - | - | - | 120.0 ± 3.0 | –38.0 ± 3.0 |
| | **2** | - | - | | 1 | - | - | - | 102.0 ± 2.6 | –32.0 ± 2.3 |

[a] Nucleation and [b] elongation constants, [c] elongation temperature, [d] degree of cooperativity, elongation [e] enthalpy and [f] entropy, and [g] nucleation enthalpy of the polymerization process calculated by decreasing $T$. [h] $m$ parameter, [i] Gibbs free energy, and [j] degree of cooperativity of the depolymerization process analyzed by increasing $\chi_D$.

In toluene (Figures 3a,c and S2A), a monomer–dimer equilibrium is established for both **1** and **2**, with clear isosbestic points at 520, 554, and 589 nm. At the same concentration, the two compounds display similar spectral features and temperature trends, which supports the notion that the same self-assembled species is formed. Both molecules showed sigmoidal temperature-dependent curves characteristic of isodesmic or equal-*K* processes. The corresponding $\alpha/T$ plots (inset in Figure 3a and Figure S4) afforded the melting temperature ($T_m$; defined as the temperature at which $\alpha = 0.5$) at each concentration, which is also indicated in Figure 3c. All the temperature-dependent data obtained in toluene were fitted to an equal-*K* model in order to calculate the main thermodynamic parameters, namely the equilibrium constant ($K_D$) and the enthalpic ($\Delta H$) and entropic changes ($\Delta S$), associated to this supramolecular process (Table S1). The data was consistent with a dimerization process and indicated a slightly stronger association for **1** ($K_D = 1.5 \times 10^4$ M$^{-1}$) than for **2** ($K_D = 4.2 \times 10^3$ M$^{-1}$) at a $3.9 \times 10^{-6}$ M concentration in toluene.

In MCH, on the contrary and as stated above, **1** and **2** displayed very different spectra, that were assigned to the head-to-tail stacks of **1** (Figures 3b,d and S2B) and the tail-to-tail dimer of **2**. Both species exhibit extraordinary stability to temperature changes and full dissociation could only be observed at high temperatures in very diluted samples (*ca.* $10^{-6}$ M). Therefore, we were limited to a very narrow concentration range to acquire complete polymerization data through cooling experiments (higher concentrations did not result in complete depolymerization, whereas lower concentrations were out of our UV-vis absorbance detection limit). Still, the polymerization mechanism for **1** at $2.5 \times 10^{-6}$ was analyzed by fitting the non-sigmoidal cooling curves obtained at 576 nm to the cooperative model developed by Meijer and co-workers,[27,28] in which the polymerization process is divided in a nucleation and an elongation phase. A non-linear least-square analysis (equations 1-3) of the experimental melting curves allowed us to obtain a set of thermodynamic parameters (Figure S5, Table 1) including: the elongation temperature ($T_e$; the temperature at which the elongation phase from the nucleus is triggered), the elongation enthalpy ($\Delta H^0$) and entropy ($\Delta S^0$), the nucleation enthalpy ($\Delta H_n^0$), the nucleation ($K_n$) and elongation ($K_e$) equilibrium constants and, finally, the degree of cooperativity ($\sigma$) associated with the polymerization process.

$$K_n = e^{\left(\frac{-(\Delta H^0 - \Delta H_n^o) - T\Delta S^o}{RT}\right)} \quad (1)$$

$$K_e = e^{\left(\frac{-(\Delta H^0 - T\Delta S^o)}{RT}\right)} \quad (2)$$

$$\sigma = \frac{K_n}{K_e} = e^{\left(\frac{\Delta H_n^o}{RT}\right)} \quad (3)$$

The data fitted reasonably well to a nucleus comprising two **1** molecules that then grows by successive SubPc head-to-tail polymerization. Our results, in particular the calculated cooperativity factors, are within the same range of those obtained from related $C_3$-symmetric planar discotics to which this model has been applied,[29] such as benzene-1,3,5-tricarboxamides (BTAs),[30] triangular-shaped oligo(phenylene ethynylene)-based trisamides,[31] disks based on the 3,3′-diamino-2,2′-bipyridine fragment,[32] or tricarboxamides,[33,34] as well as other π-conjugated molecules, such as oligo(phenylene-ethynylene)s,[35] N-heterotriangulenes[36,37] and star-shaped oligo(p-phenylene-vinylene) substituted hexaarylbenzenes.[38]

*Concentration-dependent measurements.* Next, we performed concentration-dependent absorption measurements in toluene and MCH (Figures 4a,b and S6) and the changes observed at 580 nm were plotted as a function of concentration (Figure 4c). A comparable trend to the temperature-dependent experiments was noticed when decreasing concentration: whereas in toluene both **1** and **2** dimers gradually evolved to the monomeric form through similar isosbestic points to those found in the cooling experiments (520, 554, and 589 nm), in MCH the **1** polymer and the **2** dimer showed no significant dissociation along the whole concentration range, indicating a much stronger aggregation in this aliphatic solvent.

The dilution data in toluene was fitted to a dimer model that assumes only dimer formation[39]

$$2M \overset{K_D}{\leftrightarrow} \mathrm{D} \quad (4)$$

the equilibrium constant $K_D$ can be characterized by the equation 5:

$$K_D = \frac{C_D}{(C_M)^2} \quad (5)$$

Herein, both $C_D$ (dimer concentration) and $C_M$ (monomer concentration) can be expressed as a function of the overall concentration ($C_T$) and the molar fraction of aggregated molecules ($\alpha_{agg}$) as shown in the following equations:

$$c_D = \frac{c_T \alpha_{agg}}{2} \quad (6)$$

$$c_M = c_T\left(1 - \alpha_{agg}\right) \quad (7)$$

Since the $\alpha_{agg}$ values at a certain concentration $C_T$ can be extracted from the nonlinear least-squares analysis, both $C_D$ and $C_M$ are obtainable. The resultant dimerization constants ($K_D$) calculated from the monomer absorption maximum at 580 nm are $K_D = 4.0 \pm 0.9 \times 10^4$ M$^{-1}$ for **1** and $K_D = 3.4 \pm 0.5 \times 10^3$ M$^{-}$

[1] for **2**. These values are in good agreement with the temperature dependent data in toluene and indicate again that **1** undergoes a slightly stronger dimerization process than **2** (see also the $^1$H NMR dilution measurements described below).

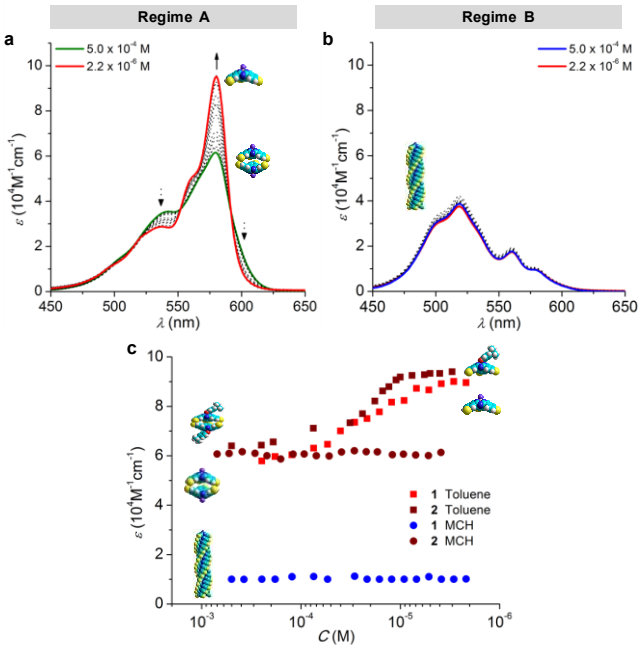


**Figure 4**. (a,b) **1** *Q*-band absorption changes as a function of the concentration in (a) toluene or (b) MCH. Arrows indicate spectral changes upon dilution. (c) Absorption changes monitored at 580 nm in toluene or MCH of **1** or **2** solutions upon dilution. In all cases, $T = 20$ °C. In red: *Regime A*. In blue: *Regime B*. The corresponding set of spectra for **2** can be found in Figure S6.

*Solvent-dependent measurements.* The dissociation of both dimer and polymer species was also monitored and analyzed by changing solvent composition. Concretely, we studied the degree of aggregation of the **1** polymer and the **2** dimer in MCH by increasing the volume fraction of 1,4-dioxane (Figure 5). The denaturation curves of **1** or **2** in MCH with 1,4-dioxane ($3.2 \times 10^{-5}$ M) were analyzed by an extended nucleation-elongation model developed by de Greef, Meijer, and co-workers (SD model).[40,33,41] In this equilibrium model the monomer addition steps in the nucleation regime are described by an equilibrium nucleation constant $K_n$ with a cooperative parameter ($\sigma$):

$$\sigma = \frac{K_n}{K_e} < 1 \qquad (8)$$

The elongation equilibrium constant $K_e$ is defined *via*:

$$K_e = e^{\left(\frac{-\Delta G^{0\prime}}{RT}\right)} \qquad (9)$$

where $\Delta G^{0\prime}$ is the Gibbs free energy gain upon monomer addition, $R$ the gas constant and $T$ the temperature. According to denaturation models, the Gibbs free energy is assumed to be linearly dependent on the volume fraction of good solvent ($\chi_D$):

$$\Delta G^{0\prime} = \Delta G^0 + m \cdot f \qquad (10)$$

where $\Delta G^0$ represents the Gibbs free energy gain upon monomer addition in the pure solvent (MCH) and the dependence of $\Delta G^{0\prime}$ on $\chi_D$ is described by the $m$ parameter, which characterizes the ability of the good solvent to associate with the monomer thereby destabilising the supramolecular aggregated species (Table 1).

SubPc **2** in MCH reveals absorption changes upon denaturation with dioxane that are typical of those observed in *Regime A*, with isosbestic points at 544 and 590 nm (Figure 5a). The degree of aggregation displays a sigmoidal dependency with dioxane content at a constant concentration and the data was fitted to the model with $\sigma = 1$ (Figure 5c), thus in accordance with the presence of a monomer-dimer equilibrium in mixtures of these solvents. The free energy gain was calculated in this case as $\Delta G^0 = -32.0 \pm 2.3$ kJ mol$^{-1}$. Likewise, **1** or **2** tail-to-tail dimer solutions in toluene developed the same spectroscopic changes as those seen in temperature- and concentration-dependent measurements when dissociated with increasing amounts of dioxane (Figure S7).

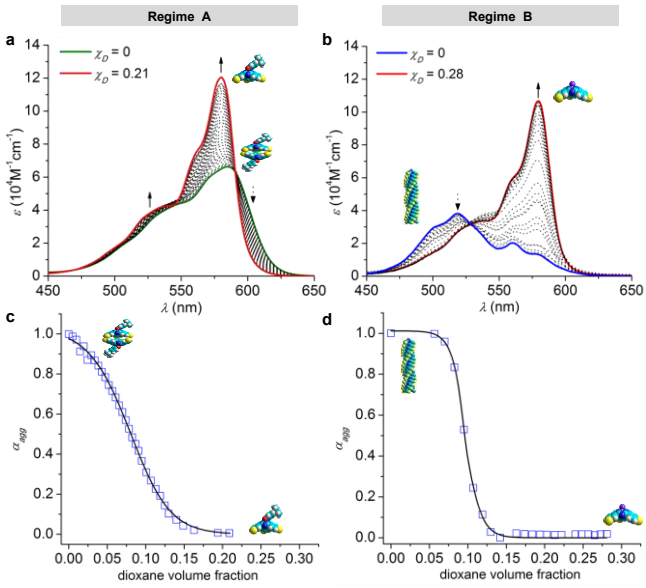


**Figure 5**. Changes in the (a) **2** and (b) **1** *Q*-band absorption spectra as a function of the volume fraction of dioxane ($\chi_D$) in MCH ($3.2 \times 10^{-5}$ M, $T = 20$ °C). Arrows indicate spectral changes upon molar fraction of dioxane increase. Fitting of denaturation curve of (c) **2** at 580 nm and (d) **1** at 519 nm to the extended nucleation-elongation model.

However, the experimental data for the self-assembly of **1** reveals a critical solvent composition in which polymerization is abruptly triggered, with a clear isosbestic point at 528 nm (Figure 5b). This fact can be attributed again to a nucleation phenomenon operating in a cooperative aggregation process.[42] Curve fitting by applying a global nonlinear least-squares procedure using the SD equilibrium model shows a good description of the data for supramolecular polymers growing *via* a cooperative mechanism (Figure 5d) with $\Delta G^0 = -38.0 \pm 3.0$ kJ mol$^{-1}$ and $\sigma = 0.027$.

**Additional Insights into the Self-assembly and Structure of the Tail-to-Tail Dimer Obtained by NMR Spectroscopy.** In order to gain a deeper insight into the self-assembly process and the structure of the associated species, we performed a series of $^1$H and $^{19}$F NMR experiments in different solvents as a function of sample concentration and temperature.

In THF-$d_8$, a solvent chosen as the NMR substitute for dioxane, **1** and **2** showed characteristic signals corresponding to

the monomeric species that did not change significantly in shape or position with temperature or concentration. The amide proton signal, presumably coordinated to solvent molecules, was found at 9.7 ppm (Figure S8A).

In chlorinated solvents like $CDCl_3$ or $CDCl_2CDCl_2$, however, **1** and **2** displayed clear signs of aggregation. Both compounds exhibited similar trends when increasing sample concentration (Figures S8B) or decreasing the temperature (Figure 6a,b): in $^1$H NMR (Figures S8B and 6a) the amide signal shifts downfield and the aromatic signals shift upfield, whereas in $^{19}$F NMR (Figure 6b) the fluorine signal of **1** broadens and experiences a downfield shift. This behavior is characteristic of a fast exchange between the monomer and a H-bonded aggregated species which, in view of the similarity between SubPcs **1** and **2**, was assigned again to the tail-to-tail dimer. On the other hand, below $10^{-4}$ M, at concentrations where optical measurements are carried out, the spectra obtained in these chlorinated solvents are typical of monomeric species. The chemical shift changes of some selected protons as a function of concentration fitted adequately to the dimer model[39] described above. In this way, the dimerization constant in $CDCl_3$ was calculated as $K_D$ = 101 ± 18 $M^{-1}$ for **1** and $K_D$ = 63 ± 13 $M^{-1}$ for **2** (see Figure S8B and Table S2).

Decreasing solvent polarity to toluene-$d_8$, however, resulted in totally different spectra (Figures 6c,d and S8C). At high temperatures, the spectra of **1** and **2** are reminiscent to those found in chlorinated solvents, but decreasing the temperature below a certain value – that depends on the sample concentration (see Figure S8C) – results in the stabilization of a self-assembled species which, surprisingly, loses the $C_3$-symmetry of the SubPc monomer. As shown in Figure 6c,d for a 5 mM sample of SubPc **1**, both $^1$H and $^{19}$F NMR reveal a clear transition around 348 K. Above that temperature, a fast exchanging monomer-dimer mixture with a single set of proton signals is found, just like in chlorinated solvents. Below that temperature and down to 238 K, an aggregated species is kinetically stabilized that presents three well-resolved sets of $^1$H signals (named hereafter with the subscripts *1*, *2* and *3*) and one set of $^{19}$F signals. These signals integrate equally at different concentrations and temperatures, suggesting the persistence of a single structure with $C_1$-symmetry below the transition temperature. All aromatic signals are strongly shifted downfield when compared to the monomer signals. In addition, the shape and position of the amide proton signals of the new species suggest that all of them are in average involved in H-bonding, but with different strength and/or chemical environment. Decreasing the temperature down to 238 K produces a downfield shift of these amide signals that is particularly evident for the $\boldsymbol{a_2}$ proton ($\Delta\delta(\boldsymbol{a_1})$ = –0.4 ppm; $\Delta\delta(\boldsymbol{a_2})$ = –1.2 ppm; $\Delta\delta(\boldsymbol{a_3})$ = –0.1 ppm), which can be an indication of the formation of stronger H-bonds. In $^{19}$F NMR experiments performed for **1** at the same concentration and in the same temperature range, a new signal arises below 348 K, again in slow exchange at the NMR timescale, that grows at the expense of the original signal found at high temperatures (see Figure 6d). The addition of very small amounts of THF-$d_8$ (below 5% v/v) produces full dissociation and the recovery of the $C_3$-symmetric proton pattern. Together with the dependence of the transition temperature with concentration (see Figure S8C), this confirms the supramolecular nature of the species formed in toluene-$d_8$. It is important to note that **2** revealed very similar $^1$H NMR changes in the same conditions and temperature range.

In order to assign all proton signals, Heteronuclear Multiple-Quantum Correlation (HMQC) $^1$H–$^{13}$C NMR experiments were performed (Figure 7a). Those signals that did not show correlation to any carbon nucleus were assigned to the amide signals. Upon addition of $D_2O$ to the sample in toluene-$d_8$ those amide signals disappeared, thus corroborating our assignment.

On the other hand, NOESY experiments afforded further useful information about the structure of the stable assembly formed in toluene and, more concretely, about the conformation of each of the three amide groups in the assembled species and hence on the origin of the loss of the $C_3$-symmetry. The amide conformations in SubPcs **1** and **2** can be divided in four groups depending on the C–C–N–H dihedral angle formed between the amide group and the isoindole ring (Figure 7b).[16] We can define *syn* and *anti* orientations, depending whether the amide carbonyl dipole is aligned parallel or antiparallel, respectively,

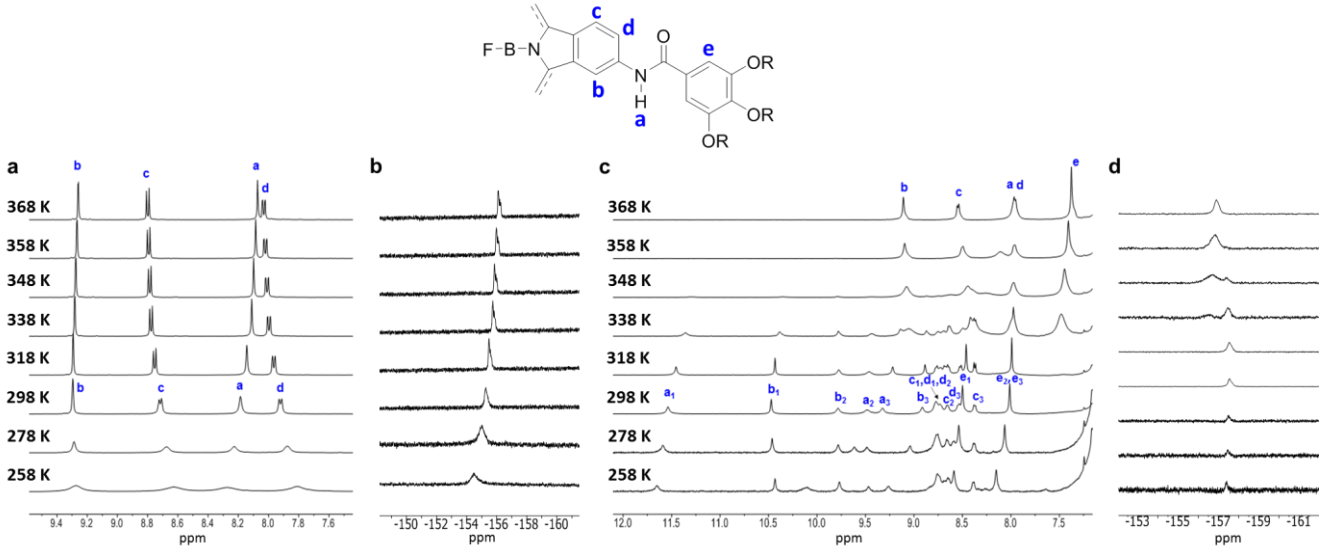


**Figure 6.** Changes in (a,c) the aromatic region of the $^1$H NMR spectrum or (b,d) the $^{19}$F NMR spectrum of **1** in (a,b) $CDCl_2CDCl_2$ and (c,d) toluene-$d_8$ as a function of temperature. In all cases: [**1**] = 5 mM (see also Figure S8C).

to the axial B−F bond, or *in* and *out* orientations, as a function of the position of the carbonyl oxygen with respect to the isoindole ring.

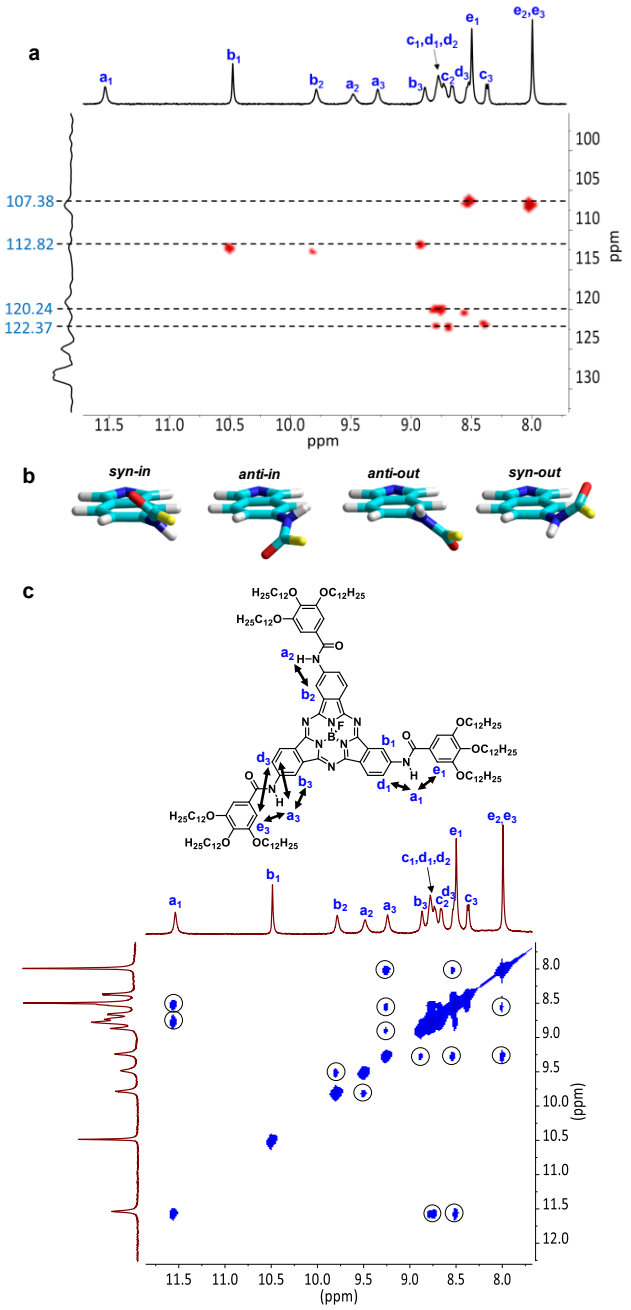


**Figure 7.** (a) HMQC NMR experiment (500 MHz; 298 K; [**1**] = 5 mM; toluene-$d_8$) showing the $^1$H–$^{13}$C correlations and the assignment of each aromatic proton signal. (b) Four groups of amide conformations that lead to intermolecular H-bonding. We can define *syn* and *anti* orientations – depending whether the amide carbonyl dipole is aligned parallel or antiparallel, respectively, to the axial B–F bond –, and *in* and *out* orientations – as a function of the position of the carbonyl oxygen (in red) with respect to the isoindole ring. (c) SubPc **1** structure and assignment of the most relevant NOE cross-peaks observed in the aromatic region of the NOESY spectrum of a 5 mM **1** solution in toluene-$d_8$ at 298 K.

Figure 7c shows the most relevant region of the NOESY spectrum of **1** in toluene-$d_8$ at 298 K, where the three signals for each aromatic and amide protons are located. Let us first focus on the amide $\boldsymbol{a_1}$ signal at 11.58 ppm. This proton displays NOE cross-peaks with the proton of one of the gallic wedges and with a vicinal proton at the β isoindole position, assigned arbitrarily as $\boldsymbol{e_1}$ and $\boldsymbol{d_1}$ (Figure 7b), but not with a "*b*" proton. This suggests an *out* orientation for this amide group. The α isoindole proton labelled as $\boldsymbol{b_1}$ in Figure 7b, which displays an unusual downfield shift, does not show NOE with any other proton and thus could belong to the same isoindole unit as amide $\boldsymbol{a_1}$ (see below). The NOE pattern is however totally different for the $\boldsymbol{a_2}$ amide proton at 9.48 ppm. This proton presents instead strong NOE cross-peaks with the α isoindole proton *ortho* to the amide group, labelled as $\boldsymbol{b_2}$, and no cross peaks with the corresponding "*d*" protons at the β isoindole position. This suggests an *in* conformation for this amide group. Finally, the amide proton at 9.28 ppm, labelled as $\boldsymbol{a_3}$ in Figure 7b, presents NOE cross-peaks with the two *ortho* protons: $\boldsymbol{b_3}$ and $\boldsymbol{d_3}$, so its conformation cannot be clearly assigned. In any case, these NOESY experiments clearly reveal that the assembled species exhibits different defined conformations for the H-bonded amide groups, and this must be the origin of the loss of the $C_3$-symmetry.

In order to confirm that the aggregates formed in toluene are compatible with the size expected for a dimer model (about 5 nm in diameter), DOSY NMR experiments were carried out in this aromatic solvent at different concentrations (Figure S8D). From these experiments, it is inferred that: 1) the diffusion-ordered signals are relatively sharp, which is characteristic of discrete assemblies, 2) all signals assigned to the dimeric assembly have the same diffusion coefficient, and 3) the analysis of the diffusion data according to the Stokes-Einstein equation revealed that the hydrodynamic radius of our assemblies in toluene is about 2.8 nm, which is in agreement with the one estimated from theoretical models (see Figure S8D). This evidence, together with the well-defined $^1$H NMR spectra, discards the formation of mixtures of ill-defined oligomers, where only one or two amide groups are H-bonded, since these should give rise to far more complex spectra that would change considerably with temperature. Furthermore, a dimer assembled *via* three H-bonding points should be far more stable in diluted solutions if we consider chelate cooperative effects.[43] The inversion of these H-bonded amide groups must be, however, fast in the NMR timescale, and this must be the reason why we cannot discern between the two SubPcs in the dimer. Figure S8E offers a more detailed interpretation of this last hypothesis.

In short, all the experimental evidence obtained in toluene-$d_8$ can only be explained by the formation of a *single tail-to-tail dimeric species with $C_1$-symmetry* for both **1** and **2**, which is in full agreement with the absorption and emission experiments performed for both compounds in toluene at similar and lower concentrations, as shown above. So, what is the cause for the symmetry loss? Why would a $C_3$-symmetric molecule associate in a $C_1$-symmetric dimer species? NOESY experiments indicated that our tail-to-tail dimer has different amide conformations. Why would they arrange in such an asymmetric fashion if a $C_3$-symmetric H-bonding arrangement is in principle allowed? Solvents with low dielectric constants, like toluene, are not suited to stabilize polar structures. Hence, we believe that the preservation of a minimum net dipole moment in the dimer, as it occurs in most crystal structures, is the reason for such striking, rarely observed unsymmetric arrangement. We can identify two main functional groups that could influence the net axial dipole moment of the **1** assemblies: i) the B−F bond, that

in a tail-to-tail dimer is canceled due to their antiparallel orientation, and ii) the amide carbonyl dipoles, which can change orientation in each isoindole unit. A $C_3$-symmetric tail-to-tail dimer with 3 H-bonded amide pairs would be able to cancel the dipole component in the *xy* plane, but never the component in the *z* direction, defined as the direction of the B−F bond. In order to cancel the *z* component as well, the H-bonded amide pairs must readapt their conformations so that the overall vector sum is zero. In short, it is obvious that a **1** tail-to-tail H-bonded dimer must adopt a distorted $C_1$-symmetric conformation to reach a minimum net dipole moment.

Finally, decreasing solvent polarity even further, by the use of cyclohexane-$d_{12}$ or mixtures of this solvent with toluene-$d_8$ resulted in the broadening of all proton signals and, at high cyclohexane-$d_{12}$ content/concentration, in the precipitation of **1**, which is consistent with a noncovalent polymerization process, as observed by optical spectroscopy at lower concentrations.

**Chiral Self-sorting in each Aggregation Regime.** With the exception of the CD spectra shown in Figure 2c, all optical and NMR spectroscopy measurements shown so far were performed with a racemic mixture of *P* and *M* SubPc enantiomers. However, these enantiomers may distribute within the two self-assembled structures, dimer and polymer, in a different manner (Figure 8). We can first distinguish between two extreme situations: i) chiral *narcissistic* self-sorting (or chiral self-recognition), leading to homochiral assemblies where each enantiomer will interact only with its own, or ii) chiral *social* self-sorting (or chiral self-discrimination), resulting in heterochiral dimers, formed by the two enantiomers, or racemic polymers, where the enantiomers alternate in the stack. In between these extreme situations, we must also consider the formation of randomly sorted polymer stacks, where there is no preference for internal order.[44]

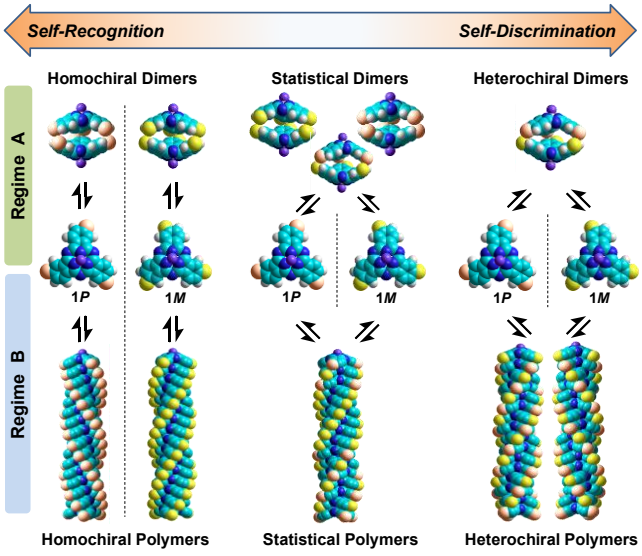


**Figure 8.** Three possible enantiomeric self-sorting situations that may occur in *Regime A* and *Regime B*: chiral self-recognition or narcissistic self-sorting (left), chiral self-discrimination or social self-sorting (right), or no self-sorting, which leads to a statistical distribution of enantiomers (middle). For a clearer differentiation between the two SubPc enantiomers, the models bear peripheral marks of different color: yellow (**1*M***) and orange (**1*P***), despite they actually represent the same chemical structure (arylamide group).

In the case of *Regime A*, for instance, three assemblies could in principle be formed (Figure 8): the homodimers **1*P*·1*P*** and **1*M*·1*M***, which have an enantiomeric relationship and would thereof give rise to a single set of proton resonances, and the "*meso*" heterodimer **1*P*·1*M*** (or **1*M*·1*P***). However, if a mixture of both homo- and heterodimers were formed in toluene (central picture in Figure 8), the $^1$H NMR spectral pattern should be more simple if both of them were $C_3$-symmetric (only 2 sets of $^1$H resonances would be observed), or far more complicated if at least one of them was $C_1$-symmetric. Moreover, both kind of dimers should present different stabilization energies and thus their relative abundance in solution should change with concentration or temperature, something that was not observed in the NMR measurements, as stated above. Therefore, chiral self-sorting must be operating in the dimerization of **1** (or **2**) in toluene, and only a single dimeric species, either a homodimer (**1*P*·1*P*** + **1*M*·1*M***) or a heterodimer (**1*P*·1*M*** / **1*M*·1*P***), is presumably formed. In the first scenario, our SubPc molecules would undergo a chiral self-recognition process (left picture in Figure 8) and, in the second scenario, a chiral self-discrimination process (right picture in Figure 8).

In order to ascertain which of these situations take place within *Regime A*, we performed identical temperature-dependent NMR analysis in toluene-$d_8$ with enantiomer **1*M***, and compared the results with those of the **1** racemate. As shown in Figure S8F, not only the same kind of three-fold splitting and shifts were observed, but also the transition temperature at which these changes were recorded is the same for both samples at the same concentration. In other words, the $^1$H NMR spectra of **1*M*** (or **1*P***) is virtually indistinguishable to that of the 1:1 racemic mixture at each temperature. This is a decisive proof that **1** undergoes a chiral self-recognition process along dimerization in *Regime A*. Nonetheless, to confirm the narcissistic self-sorting of the **1** tail-to-tail dimers, we monitored and compared the absorption and CD changes experienced by **1*P***, **1*M***, and their 1:1 mixture as a function of temperature (Figures 9a,c,e). The results, plotted in Figure 9g, indicate again that the thermodynamics of the dimerization process is virtually identical in the three cases, which is in agreement with the preferential formation of homochiral **1*P*·1*P*** + **1*M*·1*M*** dimers in the racemic mixtures.

We then turned our attention to *Regime B* in MCH. Due to the formation of polymeric assemblies with very broad $^1$H signals, a similar NMR analysis in cyclohexane-$d_{12}$ could not be made. However, the CD and absorption changes of **1*P***, **1*M***, and their 1:1 mixture could be recorded in MCH as a function of temperature (Figures 9b,d,f). As can be observed when visually comparing Figures 9d and 9f, the racemic stacks are, with a big difference, more stable than the homochiral stacks obtained from the individual enantiomers. This is also clear in the temperature-dependent trends reproduced at different concentrations in Figure 9g, from which the melting temperatures ($T_m$) were extracted. For instance, the $T_m$ of racemic polymer samples were consistently far larger than the enantiopure polymer samples, reaching differences even above 10 ºC. In addition, Table 1 compares the main thermodynamic parameters obtained by fitting the cooling curve to a nucleation-elongation process in *Regime B* for racemic and enantiopure samples. Although, as explained above, we were limited to a very narrow concentration range to fit the cooling curves with the nucleation-growth model, and thus could not compare across a wide range of concentrations, the calculated elongation temperature ($T_e$) is also significantly lower for the polymers composed of pure enantiomers when compared to the racemic mixture (Table

1). Furthermore, dissociation of the homochiral polymers required a slightly lower amount of dioxane than the stacks formed by the 1:1 mixture (Figure S9A). In short, all the experiments we performed strongly indicate that the racemic stacks (right picture in Figure 8) are more stable than those formed from single enantiomers (left picture in Figure 8), and hence that there is a clear preference for heterochiral head-to-tail binding. This means that social self-sorting, in which each enantiomer discriminates its own, mainly operates in *Regime B*.

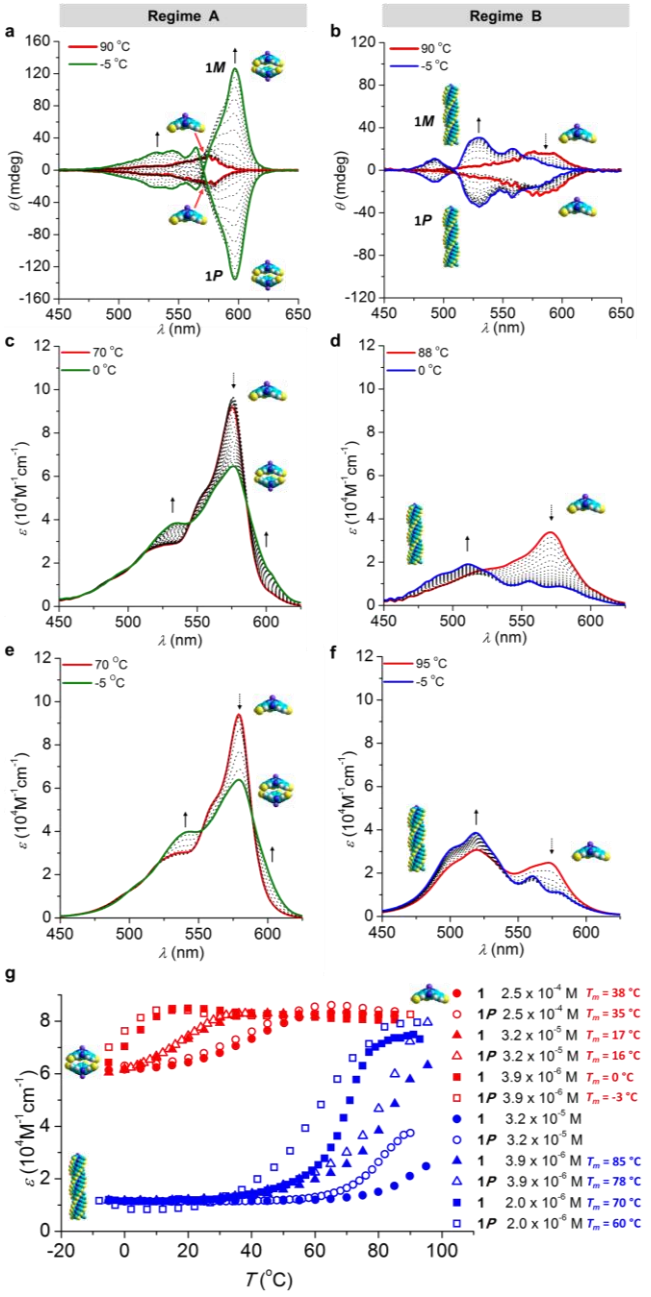


**Figure 9**. (a,b) **1*P***/**1*M*** *Q*-band CD in (a) toluene and (b) MCH solutions. **1*P*** (c,d) and **1** (e,f) absorption changes as a function of temperature in toluene (c,e) and MCH (d,f) solutions (**1*M*** absorption experiments are shown in Figure S9B). Arrows indicate the trends with decreasing temperature. [**1**] = [**1*P***] = 3.2 × $10^{-5}$ M. (**g**) Absorption changes at 580 nm as a function of temperature for racemic **1** and enantiomer **1*P*** in toluene (red) an MCH (blue) at different concentrations (see also Figure S9C).

Unfortunately, crystalline samples could not be obtained for the assemblies of **1** or **2**, or of related molecules where the long peripheral alkoxy chains are substituted with fluorine or hydrogen atoms (see compounds **3**–**6** in the S.I.), which were synthesized with the exclusive purpose to generate suitable samples for X-ray analysis. However, as will be detailed below, quantum chemical calculations were highly informative and useful to characterize and compare the structure and energetics of homochiral and heterochiral tail-to-tail dimers and head-to-tail polymers of SubPc **1**.

**Structural Models of the Tail-to-Tail Dimers and Head-to-Tail Polymers.** Theoretical calculations were performed under the density functional theory (DFT) approach and the semiempirical tight-binding GFN2-xTB model to: 1) obtain a deeper insight into the structure of the supramolecular tail-to-tail dimer and the narcissistic self-sorting behavior occurring in *Regime A*; and 2) describe the supramolecular polymer and explain the chiral self-discrimination process observed in *Regime B*.

First, tail-to-tail homochiral **1*P*·1*P*** and heterochiral **1*P*·1*M*** dimers were modelled at the DFT B97D3/6-31G** level of theory[45] without including the peripheral alkoxy chains to save computational resources (see the S.I. for full computational details). Among the different possible conformers, $C_3$-symmetric dimers (with the three pairs of amide groups equally oriented) were found to be among the most stable conformations in vacuum (see Figure 10 and Section S10 in the S.I.). The homochiral **1*P*·1*P*** $C_3$-dimer (Figure 10a) favourably interacts through a large number of noncovalent intermolecular forces between the two constituting monomers, including three strong H-bonds (1.93 Å), a mixture of π–π interactions and short CH···π interactions (2.95 Å) between the peripheral benzene rings, and a relatively close disposition of the SubPc cores (B···B distance of 6.21 Å). In contrast, the heterochiral **1*P*·1*M*** $C_3$-dimer (Figure 10b) shows slightly larger H-bonds (1.99 Å), along with an increased distance between the SubPc cores (B···B distance of 7.29 Å), and practically negligible CH···π interactions (4.06 Å). As a result, the homochiral **1*P*·1*P*** dimer is calculated 10.6 kcal $mol^{-1}$ more stable than the heterochiral **1*P*·1*M*** analogue, with binding energies ($E_{bind}$) of –60.7 and –50.2 kcal $mol^{-1}$, respectively, supporting the chiral self-recognition behaviour recorded experimentally in the dimeric *Regime A*.

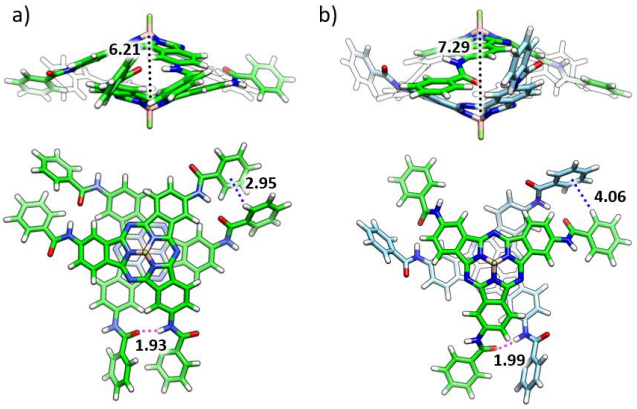


**Figure 10**. Side and top views of the minimum-energy structures calculated at the B97D3/6-31G** level of theory for the most stable tail-to-tail $C_3$ **1*P*·1*P*** homochiral (a) and **1*P*·1*M*** heterochiral (b) dimers. Characteristic intermolecular distances are indicated in Å. Carbon atoms of **1*P*** and **1*M*** are represented in green and light-blue, respectively.

The theoretical CD spectrum was calculated for the homochiral **1*P*·1*P*** dimer at the DFT level (see the SI for details). A clear intense, positive-to-negative CD signal is predicted around 500–600 nm for **1*P*·1*P*** (Figure S10Ba), which corresponds to the electronic transitions to the $S_{6/7}$ and $S_{3/4}$ singlet excited states, respectively. These transitions are described by monoelectronic local excitations involving each monomeric SubPc core in the tail-to-tail dimer (Figure S10Bb). The larger intensity and red-shift predicted for this bisignated CD band compared to the one calculated for a head-to-tail homochiral **1*P*** oligomer (Figure S10Ba),[16] supports the experimental observations (Figure 2c).

To further explain the origin of the asymmetry observed in the proton signals recorded in the $^1$H NMR experiments in toluene-$d_8$, $C_1$-**1*P*·1*P*** homochiral dimers were modelled. B97D3/6-31G** calculations indicate that $C_1$-**1*P*·1*P*** dimers (Figure S10C) can compete in energy with the most stable $C_3$-structure shown in Figure 10a, the former being less stable by only 1 kcal mol (Table S3). In the $C_1$-**1*P*·1*P*** dimers, the three amide groups of each monomer are not in the same *in*/*out* orientation with respect to the adjacent isoindole moiety and give rise to asymmetric H-bond pairs and also to asymmetric interactions between the peripheral benzene rings. This leads to a displacement of one SubPc core with respect to the other (Figure S10C), and could explain the 3 sets of $^1$H signals recorded in the NMR spectra in toluene.

On the other hand, intrigued by the clear experimental differences observed for the homochiral and heterochiral head-to-tail supramolecular polymerizations in MCH (Figure 9g), theoretical calculations were performed to give insight into the structure of the resulting supramolecular aggregate and explain the chiral self-discrimination process occurring in *Regime B* for racemic **1**. Different helical head-to-tail hexamer aggregates were constructed including the long aliphatic alkyl chains, and were fully optimized within the cost-effective GFN2-xTB method in solution (see the S.I.).[46]

Figure 11 displays the structure computed for the optimized homochiral and heterochiral (*i.e.*, alternated) hexamer stacks. For the homochiral **1*P*** hexamer (Figure 11a), a $C_3$-symmetric helical right-handed columnar assembly governed by H-bonding and strengthened by π–π, alkyl-alkyl, and dipolar electrostatic interactions is obtained. Neighboring molecules are separated by 4.20 Å and rotated by 25°. The amide groups are twisted out of the plane of the isoindole rings by 30° to promote the intermolecular H-bonds with distances around 1.9–2.1 Å. Short intermolecular C···C contacts between the isoindole rings and between the terminal benzenes of adjacent molecules are predicted in the range of 3.4–3.8 Å, indicative of the presence of attractive π–π interactions. Similarly, short H···H contacts in the 2.7–3.1 Å range are also found between the alkyl chains of neighboring molecular units. An intermolecular distance of 2.75 Å is calculated between the F and B atoms of contiguous molecules, which is significantly shorter than the sum of the van der Waals radii of boron (1.92 Å) and fluorine (1.47 Å), indicative of a strong dipolar electrostatic interaction between the B−F dipoles along the assemblies. All these values agree with the geometry parameters previously reported at the wB97X-D/cc-pVTZ level of theory.[16] Moreover, note the good accord obtained in the bisignated CD band predicted theoretically (Figure S10B) and recorded experimentally (Figure 2c) for the head-to-tail assembly.

Unlike the homochiral aggregate, where only a molecular building block (enantiomer) is self-assembled, the heterochiral aggregate can be seen as a supramolecular growth of a head-to-tail **1*P*·1*M*** heterochiral dimer (Figure 11b). This head-to-tail heterochiral dimer building block is characterized by a separation between the adjacent SubPc molecules of 4.21 Å and rotated by *ca.* 35°. Note that the amide groups are linked to different positions of the isoindole rings although the amide conformation is the same in both enantiomers. The twisting of the amide groups in each arm with respect to the plane of the isoindole rings leads to the formation of a zig-zag array of strong intermolecular H-bonds of 1.8–2.2 Å. Importantly, an efficient interaction between the peripheral long aliphatic chains of vicinal monomers with H···H contacts of 2.4–2.6 Å is predicted. Short intermolecular π–π interactions between the aromatic rings are also obtained with distances in the 3.3–3.9 Å range. The heterochiral dimer can therefore grow up supramolecularly by forming a $C_3$-symmetric head-to-tail helical columnar assembly of heterochiral subunit pairs, which is stabilized, similarly to its homochiral homologue (Figure 11a), by H-bonds and π–π, alkyl-alkyl, and dipolar electrostatic interactions.

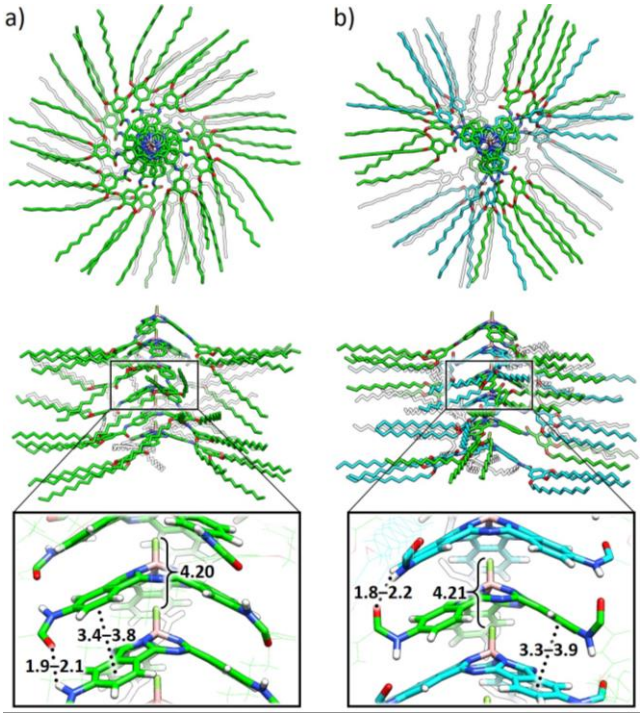


**Figure 11**. Top and side views of the $C_3$-symmetry-like helical homochiral (a) and heterochiral (b) fully-optimized hexamers calculated at the GFN2-xTB level of theory. Carbon atoms of **1*P*** and **1*M*** enantiomers are represented in green and light-blue, respectively.

In terms of energetics, the $C_3$-symmetric head-to-tail helical heterochiral hexamer turns out to be the most stable aggregate, with a total energy difference of ca. 23 kcal/mol with respect to its homochiral analogue (*ca.* 5 kcal/mol per interacting pair). This theoretical outcome stems from the more efficient core-to-core interaction and the larger amount of aliphatic contacts between vicinal peripheral alkyl chains, as mentioned above. Our calculations therefore suggest that, in the presence of a racemic mixture of **1**, the formation of a helical heterochiral supramolecular polymer would be energetically favored against a homochiral polymer, thus in agreement with the self-discrimination process experimentally observed in this regime.

## CONCLUSIONS

This work demonstrates that reducing the symmetry of a π-conjugated discotic from the classical planar $D_n$ to a conic $C_n$ introduces novel intermolecular binding modes that can generate richer self-assembly landscapes. In particular, by providing a cone-shaped SubPc molecule with the classical peripheral arylamide "sticky" groups, we have proven that two association modes, defined by the establishment of either convex-concave (head-to-tail) or concave-concave (tail-to-tail) intermolecular interactions, exist exclusively within two distinct regimes. These regimes are only defined by the solvent nature, either aliphatic or aromatic, and we never observed any "foreign" self-assembled species in neither of them, independently on sample temperature or concentration.

In toluene, SubPc **1** undergo a tail-to-tail dimerization process by establishing three H-bonds between arylamide units, which is characterized by a sigmoidal monomer-dimer transition. Surprisingly, at relatively low temperatures the structure of the dimer becomes very well-resolved by $^1$H NMR, which reveals that each isoindole unit presents different conformations, leading to the loss of the $C_3$-symmetry. This rarely observed phenomenon was attributed to the requirement to maintain a null net dipole moment in the dimer structure within the nonpolar solvent matrix, as it happens in many crystal structures. A comparison between the self-assembly of racemic **1** and enantiopure **1*M*** /**1*P*** by temperature dependent NMR and UV measurements disclosed a marked narcissistic self-sorting behavior. This means that each of the enantiomers in the racemate prefers to associate with itself, leading to homochiral dimer structures. Computational calculations supported this experimental finding. Homochiral dimers were found to be substantially more stable than their heterochiral versions and, in addition, reproduced quite well the sign of the experimental CD spectrum.

In MCH the supramolecular scenario changes radically, and SubPc **1** is found to associate in a head-to-tail mode, which leads to non-centrosymmetric columnar polymers, as it was also previously observed in homochiral samples and in lyotropic or thermotropic liquid crystals.[9,10,16] The most likely explanation is that aliphatic solvents are far less efficient in solvating π-conjugated moieties, and the concave-convex polymeric association clearly leaves a minimum amount of exposed π-surfaces. Such polymers are formed from the monomer through a cooperative nucleation-growth mechanism, as determined in temperature- and solvent-dependent measurements. Interestingly, the **1** racemate columnar polymers were found to be substantially more stable than homochiral **1*M*** /**1*P*** polymers, which suggests that **1*M*** and **1*P*** tend to alternate, or socially self-sort, along the stack. Theoretical calculations, which are able to predict the experimental CD sign from a homochiral structure, indicate that the reason behind this preference resides in the stronger core-to-core contacts of head-to-tail heterochiral stacks in comparison to the homochiral versions. Hence, this work additionally constitutes a nice example of how different can be the self-assembly of enantiopure and racemic samples for molecules in which the chiral center resides at the aromatic core and not at the peripheral chains, as also observed by other authors.[39,41a,47,48]

## ASSOCIATED CONTENT

**Supporting Information**. Experimental procedures and compound characterization data, along with Figures S1–S10 and Tables S1–S3. This material is available free of charge via the Internet at http://pubs.acs.org.

## AUTHOR INFORMATION


### Corresponding Author

enrique.orti@uv.es
tomas.torres@uam.es
david.gonzalez.rodriguez@uam.es


### Author Contributions

All authors have given approval to the final version of the manuscript.


## ORCID

David González-Rodríguez: 0000-0002-2651-4566

María J. Mayoral: 0000-0001-7156-5939

Fátima Aparicio: 0000-0002-4237-3011

Tomás Torres: 0000-0001-9335-6935

Enrique Ortí: 0000-0001-9544-8286

Juan Aragó: 0000-0002-0415-9946

Joaquín Calbo: 0000-0003-4729-0757



## ACKNOWLEDGMENT

Funding from the Spanish MINECO/MCIU [PGC2018-099568-B-I00, CTQ2017-85393-P, CTQ2017-84727-P, ERA-NET/European Commission/MINECO (UNIQUE, SOLAR-ERA.NET Cofund 2 N° 008/ PCI2019-111889-2), and RED2018-102331-T], the Generalitat Valenciana (SEJI/2018/035), and European Feder funds (PGC2018-099568-B-I00) is gratefully acknowledged. IMDEA Nanociencia acknowledges support from the "Severo Ochoa" Programme for Centres of Excellence in R&D (MINECO, Grant SEV2016-0686). F.A. is grateful to MSCA-COFUND InterTalentum (713366) and MSCA-IF (793506) programs. J.A. is grateful to MCIU for a "Ramon-y-Cajal" fellowship (RyC-2017-23500).


## REFERENCES


(1) Wang, L.; Huang, D.; Lam, L.; Cheng, Z. Bowlics: history, advances and applications. *Liquid Crystals Today*, **2017**, *26*, 85–111.

(2) For excellent reviews on columnar liquid crystals see: (a) Sergeyev, S.; Pisula, W.; Geerts, Y. H. Discotic liquid crystals: a new generation of organic semiconductors. *Chem. Soc. Rev*. **2007**, *36*, 1902–1929. (b) Laschat, S.; Baro, A.; Steinke, N.; Giesselmann, F.; Hägele, C.; Scalia, G.; Judele, R.; Kapatsina, E.; Sauer, S.; Schreivogel, A.; Tosoni, M. Discotic Liquid Crystals: From Tailor-Made Synthesis to Plastic Electronics. *Angew. Chem. Int. Ed*. **2007**, *46*, 4832–4887. (c) Kaafarani, B. R. Discotic Liquid Crystals for Opto-Electronic Applications. *Chem. Mater*. **2011**, *23*, 378–396. (d) Wöhrle, T.; Wurzbach, I.; Kirres, J.; Kostidou, A.; Kapernaum, N.; Litterscheidt, J.; Haenle, J. C.; Staffeld, P.; Baro, A.; Giesselmann, F.; Laschat, S. Discotic Liquid Crystals. *Chem. Rev*. **2016**, *116*, 1139−1241.

(3) (a) Pisula, W.; Feng, X.; Müllen, K. Tuning the Columnar Organization of Discotic Polycyclic Aromatic Hydrocarbons. *Adv. Mater*. **2010**, *22*, 3634–3649. (b) Kumar, S. Chemistry of Discotic Liquid Crystals. From Monomers to Polymers. CRC Press. Taylor & Francis Group.: New York, 2011. (c) Gupta, R. K.; Sudhakar, A. A. Perylene-Based Liquid Crystals as Materials for Organic Electronics Applications. *Langmuir* **2019**, *35*, 2455. (d) Kim, Y.-K.; Noh, J.; Nayani, K.; Abbott, N. L. Soft matter from liquid crystals. *Soft Matter* **2019**, *15*, 6913.

(4) (a) Hoeben, F. J. M.; Jonkheijm, P.; Meijer, E.W.; Schenning, A. P. H. J. About Supramolecular Assemblies of π-Conjugated Systems. *Chem. Rev*. **2005**, *105*, 1491–1546. (b) González-Rodríguez, D.; Schenning, A. P. H. J. Hydrogen-bonded Supramolecular π-Functional Materials. *Chem. Mater*. **2011**, *23*, 310–325. (c) Aida, T.; Meijer, E. W.; Stupp, S. I. Functional Supramolecular Polymers. *Science*, **2012**, *335*, 813-817. (d) Babu, S. S.; Praveen, V. K.; Ajayaghosh, A. Functional π-Gelators and Their Applications. *Chem. Rev*. **2014**, 114, 1973. (e) Sorrenti, A.; Leira-Iglesias, J.; Markvoort, A. J.; de Greef, T. F. A.; Hermans, T. M. Non-equilibrium supramolecular polymerization *Chem. Soc. Rev.* **2017**, *46*, 5476. (f) Matern, J.; Dorca, Y.; Sánchez, L.; Fernández, G. Revising Complex Supramolecular Polymerization under Kinetic and Thermodynamic Control *Angew. Chem., Int. Ed.* **2019**, *58*, 16730.

(5) The term "cone-shaped discotic", or also "bowlic / pyramidic" was coined in 1985 by Zimmerman and Collet. See: (a) Zimmermann, H.; Poupko, R.; Luz, Z.; Billard, J. *Z.* Pyramidic Mesophases *Naturforsch*. **1985**, *40a*, 149–160. (b) Malthete, J.; Collet, A. Liquid-crystals with a cone-shape cyclotriveratrylene core. *Nouv. J. Chim*. **1985**, *9*, 151–153.

(6) (a) Rosen, B. M.; Wilson, C. J.; Wilson, D. A.; Peterca, M.; Imam, M. R.; Percec, V. Dendron-Mediated Self-Assembly, Disassembly, and Self-Organization of Complex Systems *Chem. Rev*. **2009**, *109*, 6275. (b) Hudson, S. D.; Jung, H.-T.; Percec, V.; Cho, W.-D.; Johansson, G.; Ungar, G.; Balagurusamy, V. S. K. Direct Visualization of Individual Cylindrical and Spherical Supramolecular Dendrimers *Science* **1997**, *278*, 449. (c) Percec, V.; Ahn, C. H.; Ungar, G.; Yeardley, D. J. P.; Möller, M.; Sheiko, S. S. Controlling polymer shape through the self-assembly of dendritic side-groups *Nature* **1998**, *391*, 161. (d) Percec, V.; Imam, M. R.; Peterca, M.; Wilson, D. A.; Graf, R.; Spiess, H. W.; Balagurusamy, V. S. K.; Heiney, P. A. Self-Assembly of Dendronized Triphenylenes into Helical Pyramidal Columns and Chiral Spheres *J. Am. Chem. Soc.* **2009**, *131*, 7662. (e) Percec, V.; Imam, M. R.; Peterca, M.; Wilson, D. A.; Heiney, P. A. Self-Assembly of Dendritic Crowns into Chiral Supramolecular Spheres *J. Am. Chem. Soc.* **2009**, *131*, 1294. (f) Peterca, M.; Imam, M. R.; Ahn, C.-H.; Balagurusamy, V. S. K.; Wilson, D. A.; Rosen, B. M.; Percec, V. Transfer, Amplification, and Inversion of Helical Chirality Mediated by Concerted Interactions of C3-Supramolecular Dendrimers *J. Am. Chem. Soc.* **2011**, *133*, 2311. (g) Sahoo, D.; Imam, M. R.; Peterca, M.; Partridge, B. E.; Wilson, D. A.; Zeng, X.; Ungar, G.; Heiney, P. A.; Percec, V. Hierarchical Self-Organization of Chiral Columns from Chiral Supramolecular Spheres *J. Am. Chem. Soc.* **2018**, *140*, 13478. (h) Wilson, D. A.; Andreopoulou, K. A.; Peterca, M.; Leowanawat, P.; Sahoo, D.; Partridge, B. E.; Xiao, Q.; Huang, N.; Heiney, P. A.; Percec, V. Supramolecular Spheres Self-Assembled from Conical Dendrons Are Chiral *J. Am. Chem. Soc.* **2019**, *141*, 6162.

(7) Sawamura, M.; Kawai, K.; Matsuo, Y.; Kanie, K.; Kato, T.; Nakamura, E. Stacking of conical molecules with a fullerene apex into polar columns in crystals and liquid crystals. *Nature* **2002**, *419*, 702–705.

(8) (a) Malthete, J.; Collet, A. Inversion of the cyclotribenzylene cone in a columnar mesophase: a potential way to ferroelectric materials. *J. Am. Chem. Soc.* **1987**, *109*, 7544–7545. (b) Miyajima, D.; Tashiro, K.; Araoka, F.; Takezoe, H.; Kim, J.; Kato, K.; Takata, M.; Aida, T. Liquid Crystalline Corannulene Responsive to Electric Field. *J. Am. Chem. Soc.* **2009**, 131, 44–45. (c) Miyajima, D.; Araoka, F.; Takezoe, H.; Kim, J.; Kato, K.; Takata, M.; Aida, T. Ferroelectric Columnar Liquid Crystal Featuring Confined Polar Groups Within Core–Shell Architecture. *Science*, **2012**, *336*, 209–213. (d) Casellas, N. M.; Urbanaviciute, I.; Cornelissen, T. D.; Berrocal, J. A.; Torres, T.; Kemerink, M.; García-Iglesias, M. Resistive switching in an organic supramolecular semiconducting ferroelectric. *Chem.Commun.* **2019**, *55*, 8828–8831.

(9) (a) Guilleme, J.; Cavero, E.; Sierra, T.; Ortega, J.; Folcia, C. L.; Etxebarria, J.; Torres, T.; González-Rodríguez, D. Polar Switching in a Lyotropic Columnar Nematic Liquid Crystal Made of Bowl-Shaped Molecules. *Adv. Mater*. **2015**, *27*, 4280-4284. (b) Gorbunov, A. V.; Garcia-Iglesias, M.; Guilleme, J.; Cornelissen, T. D.; Roelofs, W. S. C.; Torres, T.; González-Rodríguez, D.; Meijer, E. W.; Kemerink, M. Ferroelectric self-assembled molecular materials showing both rectifying and switchable conductivity. *Sci. Adv*. **2017**, *3*, e1701017.

(10) Guilleme, J.; Aragó, J.; Ortí, E.; Cavero, E.; Sierra, T.; Ortega, J.; Folcia, C. L.; Etxebarria, J.; González-Rodríguez, D.; Torres, T. A columnar liquid crystal with permanent polar order. *J. Mater. Chem. C* **2015**, *3*, 985–989.

(11) Zhang, C.; Nakano, K.; Nakamura, M.; Araoka, F.; Tajima, K.; Miyajima, D. Noncentrosymmetric Columnar Liquid Crystals with the Bulk Photovoltaic Effect for Organic Photodetectors. *J. Am. Chem. Soc*. **2020**, *142*, 3326–3330.

(12) Amaya, T.; Seki, S.; Moriuchi, T.; Nakamoto, K.; Nakata, T.; Sakane, H.; Saeki, A.; Tagawa, S.; Hirao, T. Anisotropic Electron Transport Properties in Sumanene Crystal. *J. Am. Chem. Soc*. **2009**, *131*, 408–409.

(13) (a) Takezoe, H.; Kishikawa, K.; Gorecka, E. Switchable columnar phases. *J. Mater. Chem*. **2006**, *16*, 2412–2416. (b) Horiuchi, S.; Tokura, Y. Organic ferroelectrics. *Nat. Mater*. **2008**, *7*, 357–361. (c) Takezoe, H.; Araoka, F. Polar columnar liquid crystals. *Liq. Cryst*. **2013**, *41*, 393-401. (d) Tayi, A. S.; Kaeser, A.; Matsumoto, M.; Aida, T.; Stupp, S. I. Supramolecular ferroelectrics. *Nat. Chem*. **2015**, *7*, 281–294. (e) Shoyama, K.; Schmidt, D.; Mahl, M.; Würthner, F. Electron-Poor Bowl-Shaped Polycyclic Aromatic Dicarboximides: Synthesis, Crystal Structures, and Optical and Redox Properties. *Org. Lett*. **2017**, *19*, 5328–5331. (f) Guo, Q.; Yan, K.; Chigrinov, V.; Zhao, H.; Tribelsky, M. Ferroelectric Liquid Crystals: Physics and Applications. *Crystals* **2019**, *9*, 470. (g) Nguyen, M. L.; Cho, B.-K. Ferroelectrically Switchable Axial Polarization in Columnar Liquid Crystalline Phases. *Chem. Eur. J.* **2020**, *26*, 6964 –6975. (h) Mayoral, M. J.; Torres, T.; González-Rodríguez, D. Polar columnar assemblies of subphthalocyanines. *J. Porphyrins Phthalocyanines* **2020**, 24, 33-42.

(14) (a) Shimizu, S.; Miura, A.; Khene, S.; Nyokong, T.; Kobayashi, N. Chiral 1,2-Subnaphthalocyanines. *J. Am. Chem. Soc*. **2011**, *133*, 17322–17328. (b) Markopoulos, G.; Henneicke, L.; Shen, J.; Okamoto, Y.; Jones, P. G.; Hopf, H. Tribenzotriquinacene: A Versatile Synthesis and $C_3$-Chiral Platforms. *Angew. Chem. Int. Ed*. **2012**, *51*, 12884–12887. (c) Rommelmann, P.; Nachtigall, B.; Guntelmann, T.; Gröger, H.; Kuck, D. Stereoselective synthesis of enantiomerically pure bowl-shaped hydroxytribenzotriquinacenes. *Org. Biomol. Chem.* **2018**, *16*, 5635–5642.

(15) (a) Sato, K.; Itoh, Y.; Aida, T. Homochiral supramolecular polymerization of bowl-shaped chiral macrocycles in solution. *Chem. Sci*. **2014**, *5*, 136–140. (b) Roche, C.; Sun, H.-J.; Prendergast, M. E.; Leowanawat, P.; Partridge, B.E.; Heiney, P. A.; Araoka, F.; Graf, R.; Spiess, H. W.; Zeng, X.; Ungar, G.; Percec, V. Homochiral Columns Constructed by Chiral Self-Sorting During Supramolecular Helical Organization of Hat-Shaped Molecules, *J. Am. Chem. Soc.* **2014**, *136*, 7169–7185.

(16) Guilleme, J.; Mayoral, M. J.; Calbo, J.; Aragó, J. Viruela, P. M.; Ortí, E.; González-Rodríguez, D.; Torres, T. Non-Centrosymmetric Homochiral Supramolecular Polymers of Tetrahedral Subphthalocyanine Molecules. *Angew. Chem. Int. Ed*. **2015**, *54*, 2543–2547.

(17) (a) Palmans, A. R.; Meijer, E. W. Amplification of Chirality in Dynamic Supramolecular Aggregates. *Angew. Chem. Int. Ed.* **2007**, *46*, 8948–8969. (b) Jiang, H.; Zhang, L.; Liu, M. Self-Assembly of 1D Helical Nanostructures into Higher Order Chiral Nanostructures in Supramolecular Systems. *ChemNanoMat* **2018**, *4*, 720. (c) Yue, B.; Zhu, L. Dynamic Modulation of Supramolecular Chirality Driven by Factors from Internal to External Levels. *Chem. Asian J.* **2019**, *14*, 2172. (d) Dorca, Y.; Greciano, E. E.; Valera, J. S.; Gómez, R.; Sánchez, L. Hierarchy of Asymmetry in Chiral Supramolecular Polymers: Toward Functional, Helical Supramolecular Structures. *Chem. Eur. J.* **2019**, *25*, 5848.

(18) (a) Malthete, J.; Collet, A. Inversion of the cyclotribenzylene cone in a columnar mesophase: a potential way to ferroelectric materials. *J. Am. Chem. Soc*. **1987**, *109*, 7544–7545. (b) Zimmermann, H.: Tolstoy, P.; Limbach, H.-H.; Poupko, R.; Luz, Z. The Saddle Form of Cyclotriveratrylene. *J. Phys. Chem. B*, **2004**, *108*, 18772–18778. (c) Lovas, F. J.; McMahon, R. J.; Grabow, J.-U.; Schnell, M.; Mack, J.; Scott, L. T.; Kuczkowski, R. L. Interstellar Chemistry: A Strategy for Detecting Polycyclic Aromatic Hydrocarbons in Space. *J. Am. Chem. Soc.* **2005**, *127*, 4345–4349. (d) Kang, J.; Miyajima, D.; Mori, T.; Inoue, Y.; Itoh, Y.; Aida, T. A rational strategy for the realization of

chain-growth supramolecular polymerization *Science*, **2015**, *347*, 646–651.

(19) (a) Claessens, C. G.; González-Rodríguez, D.; Torres, T. Subphthalocyanines: Singular Nonplanar Aromatic CompoundsSynthesis, Reactivity, and Physical Properties. *Chem Rev*. **2002**, *102*, 835–853. (b) Claessens, C. G.; González-Rodríguez, D.; Rodríguez-Morgade, M. S.; Medina, A.; Torres, T. Subphthalocyanines, Subporphyrazines, and Subporphyrins: Singular Nonplanar Aromatic Systems. *Chem Rev*. **2014**, *114*, 2192–2277. (c) Shimizu, S.; Kobayashi, N. Structurally-modified subphthalocyanines: molecular design towards realization of expected properties from the electronic structure and structural features of subphthalocyanine. *Chem. Commun.,* **2014**, *50***,** 6949-6966.

(20) (a) Samdal, S.; Volden, H. V.; Ferro, V. R.; García de la Vega, J. M.; González-Rodríguez, D.; Torres, T. Molecular Structure of Chloro-dodecafluorosubphthalocyanato Boron(III) by Gas-Phase Electron Diffraction and Quantum Chemical Calculations. *J. Phys. Chem. A* **2007**, *111,* 4542–4550. (b) Claessens, C. G.; González-Rodríguez, D.; Iglesias, R. S.; Torres, T. Convex-convex and concave-convex interactions between $C_{60}$ and non-planar aromatic subphthalocyanine macrocycle in both covalent and supramolecular arrays. *C. R. Chimie*, **2006**, *9*, 1094-1099. (c) González-Rodríguez, D.; Torres, T. Peripheral functionalization of subphthalocyanines. *Eur. J. Org. Chem.* **2009**, 1871-1879. (d) Guilleme, J.; Martínez-Fernández, L.; González-Rodríguez, D.; Corral, I.; Yáñez, M.; Torres, T. An insight into the mechanism of the axial ligand exchange reaction in boron subphthalocyanine macrocycles. *J. Am. Chem. Soc.* **2014**, *136*, 14289-14298.

(21) Claessens, C. G.; González-Rodríguez, D.; Torres, T.; Martín, G.; Agulló-López, F.; Ledoux, I.; Zyss, J.; Ferro, V. R.; García de la Vega, J. M. Structural Modulation of the Dipolar−Octupolar Contributions to the NLO Response in Subphthalocyanines. *J. Phys. Chem B.* **2005**, *109*, 3800–3806.

(22) Spesia, M. B.; Durantini, E. N. Synthesis and antibacterial photosensitizing properties of a novel tricationic subphthalocyanine derivative. *Dyes Pigm.* **2008**, *77*, 229-237.

(23) (a) González-Rodríguez, D.; Torres, T.; Guldi, D. M.; Rivera, J.; Herranz, M. A.; Echegoyen, L. Subphthalocyanines: Tuneable Molecular Scaffolds for Intramolecular Electron and Energy Transfer Processes. *J. Am. Chem. Soc.* **2004**, *126*, 6301–6313. (b) González-Rodríguez, D.; Torres, T.; Olmstead, M. M.; Rivera, J.; Herranz, M. A.; Echegoyen, L.; Atienza-Castellanos, C.; Guldi, D. M. Photoinduced Charge-Transfer States in Subphthalocyanine−Ferrocene Dyads. *J. Am. Chem. Soc.* **2006**, *128*, 10680-10681. (c) González-Rodríguez, D., Carbonell, E., de Miguel Rojas, G., Atienza Castellanos, C., Guldi, D. M., Torres, T. Activating Multistep Charge-Transfer Processes in Fullerene−Subphthalocyanine−Ferrocene Molecular Hybrids as a Function of π−π Orbital Overlap. *J. Am. Chem. Soc.* **2010**, *132*, 16488-16500. (d) Romero-Nieto, C.; Guilleme, J.; Fernández-Ariza, J.; Rodríguez-Morgade, M. S.; González-Rodríguez, D.; Torres, T.; Guldi, D. M. Ultrafast Photoinduced Processes in Subphthalocyanine Electron Donor–Acceptor Conjugates Linked by a Single B–N Bond. *Org. Lett.* **2012**, *14*, 5656-5659. (e) Romero Nieto, C.; Guilleme, J.; Villegas, C.; Delgado, J. L.; González-Rodríguez, D.; Martín, M.; Torres, T.; Guldi, D. M. *J. Mater. Chem.* **2011**, 21, 15914-15918. (f) Kc, C. B.; Lim, G. N.; D'Souza, F. Charge Separation in Graphene-Decorated Multimodular Tris(pyrene)–Subphthalocyanine–Fullerene Donor–Acceptor Hybrids. *Angew. Chem. Int. Ed*. **2015**, *54*, 5088 –5092. (g) Rudolf, M.; Trukhina, O.; Perles, J.; Feng, L.; Akasaka, T.; Torres, T.; Guldi, D. M. Taming C60 fullerene: tuning intramolecular photoinduced electron transfer process with subphthalocyanines. *Chem. Sci.* **2015**, *6*, 4141–4147.

(24) (a) Morse, G.E.; Bender, T. P. Boron Subphthalocyanines as Organic Electronic Materials. *ACS Appl. Mater. Interfaces*, **2012**, *4*, 5055–5068. (b) Menke, S. M.; Luhman, W. A.; Holmes, R. J. Tailored exciton diffusion in organic photovoltaic cells for enhanced power conversion efficiency. *Nature Mater.* **2012***, 12*, 152–157. (c) Cnops,K.; Rand, B.P.; Cheyns, D.; Verreet, B.; Empl, M. A.; Heremans, P. 8.4% efficient fullerene-free organic solar cells exploiting long-range exciton energy transfer. *Nature Commun*. **2014**, *5*, 3406. (d) Cnops, K.; Zango, G.; Genoe, J.; Heremans, P.; Martinez-Diaz, M. V.; Torres, T.; Cheyns, D. Energy Level Tuning of Non-Fullerene Acceptors in Organic Solar Cells. *J. Am. Chem. Soc*. **2015**, *137*, 8991−8997. (e) Josey, D. S.; Nyikos, S. R.; Garner, R. K.; Dovijarski, A.; Castrucci, J. S.; Wang, J. M.; Evans, G. J.; Bender, T. P. Outdoor Performance and Stability of Boron Subphthalocyanines Applied as Electron Acceptors in Fullerene-Free Organic Photovoltaics. *ACS Energy Lett*. **2017**, *2*, 726−732. (f) De la Torre, G.; Bottari, G.; Torres, T. Phthalocyanines and Subphthalocyanines: Perfect Partners for Fullerenes and Carbon Nanotubes in Molecular Photovoltaics. *Adv. Energy Mater*. **2017**, *7*, 1601700. (g) Duan, D.; Zango, G.; García-Iglesias, M.; Colberts, F. J. M; Wienk, M. M.; Martínez-Díaz, M. V.; Janssen, R. A. J.; Torres, T. The Role of the Axial Substituent in Subphthalocyanine Acceptors for Bulk-Heterojunction Solar Cells. *Angew. Chem. Int. Ed*. **2017**, *56*, 148 –152.

(25) The hexagonal columnar head-to-tail stacking of SubPcBF molecules was proven in monocrystalline samples. See: Rodríguez-Morgade, M. S.; Claessens, C. G.; Medina, A.; González-Rodríguez, D.; Gutierrez-Puebla, E.; Monge, A.; Alkorta, I.; Elguero, J.; Torres, T. Synthesis, Characterization, Molecular Structure and Theoretical Studies of Axially Fluoro-Substituted Subazaporphyrins. *Chem. Eur. J*. **2008**, *14*, 1342–1350.

(26) Markiewicz, G.; Smulders, M. J.; Stefankiewicz A. R. Steering the Self-Assembly Outcome of a Single NDI Monomer into Three Morphologically Distinct Supramolecular Assemblies, with Concomitant Change in Supramolecular Polymerization Mechanism. *Adv. Sci*. **2019**, 6, 1900577.

(27) (a) Maarkvort, A. J.; Ten Eikelder, H. M. M.; Hilbers, P. J. J.; De Greef, T. F. A.; Meijer, E. W. Theoretical models of nonlinear effects in two-component cooperative supramolecular copolymerizations. *Nat. Commun.* **2011**, *2*, 509. (b) Ten Eikelder, H. M. M.; Markwoort, A. J.; De Greef, T. F. A.; Hilbers, P. A. J. An Equilibrium Model for Chiral Amplification in Supramolecular Polymers. *J. Phys. Chem. B* **2012**, *116*, 5291-5301.

(28) Rest, C.; Kandanelli, R.; Fernández, G. Strategies to create hierarchical self-assembled structures via cooperative non-covalent interactions. *Chem. Soc. Rev*. **2015**, *44*, 2543-2572.

(29) Dorca, Y.; Matern, J.; Fernández, G.;,Sánchez, L. C3-symmetrical π-Scaffolds: Useful Building Blocks to Construct Helical Supramolecular Polymers. *Isr. J. Chem*. **2019**, 59, 869-880.

(30) Kulkarni, C.; Meijer, E. W.; Palmans, A. R. A. Cooperativity Scale: A Structure–Mechanism Correlation in the Self-Assembly of Benzene-1,3,5-tricarboxamides. *Acc. Chem. Res*. **2017**, *50*, 1928−1936

(31) (a) Aparicio, F.; García, F.; Fernández, G.; Matesanz, E.; Sánchez, L. Mirror Helices and Helicity Switch at Surfaces Based on Chiral Triangular-Shape Oligo(phenylene ethynylenes). *Chem. Eur. J*. **2011**, *17*, 2769-2776. (b) García, F.; Viruela, P. M.; Matesanz, E.; Ortí, E.; Sánchez, L. Cooperative Supramolecular Polymerization and Amplification of Chirality in C3-Symmetrical OPE-Based Trisamides. *Chem. Eur. J*. **2011**, *17*, 7755 –7759.

(32) García, F.; Sánchez, L. Structural Rules for the Chiral Supramolecular Organization of OPE-based Discotics: Induction of Helicity and Amplification of Chirality. *J. Am. Chem. Soc*. **2012**, *134*, 734−742.

(33) García, F.; Korevaar, P. A.; Verlee, A.; Meijer, E. W.; Palmans, A. R. A.; Sánchez, L. The influence of [small pi]-conjugated moieties on the thermodynamics of cooperatively self-assembling tricarboxamides. *Chem. Commun*. **2013**, *49*, 8674-8676.

(34) Greciano, E. E.; Calbo, J.; Buendía, J.; Cerdá, J.; Arago, J.; Ortí, E.; Sanchez, L. Decoding the Consequences of Increasing the Size of Self Assembling Tricarboxamides on Chiral Amplification. *J. Am. Chem. Soc*. **201**9, 141, 7463−7472.

(35) Wang, F.; Gillissen, M. A. J.; Stals, P. J. M.; Palmans, A. R. A.; Meijer, E. W. Hydrogen Bonding Directed Supramolecular Polymerisation of Oligo(Phenylene-Ethynylene)s: Cooperative Mechanism, Core Symmetry Effect and Chiral Amplification. *Chem. Eur. J.* **2012**, *18*, 11761-11770.

(36) Valera, J. S.; Gómez, R.; Sánchez, L. Tunable Energy Landscapes to Control Pathway Complexity in Self-Assembled N-Heterotriangulenes: Living and Seeded Supramolecular Polymerization. *Small* **2018**, 14, 1702437.

(37) Valera, J. S.; Sánchez-Naya, R.; Ramírez, F. J.; Zafra, J. L.; Gómez, R.; Casado, J.; Sánchez, L. Solvent-Directed Helical Stereomutation Discloses Pathway Complexity on N-Heterotriangulene-Based Organogelators. *Chem.Eur.J.* **2017**, 23, 11141 –11146.

(38) Tomovic, Z.; van Dongen, J.; George, S. J.; Xu, H.; Pisula, W.; Leclère, P.; Smulders, M. M. J.; De Feyter, S.; Meijer, E. W.; Schenning, A. P. H. J. Star-Shaped Oligo(p-phenylenevinylene) Substituted Hexaarylbenzene: Purity, Stability, and Chiral Self-assembly. *J. Am. Chem. Soc*. **2007**, *129*, 16190-16196.

(39) Shao, C.; Grüne, M.; Stolte, M.; Würthner, F. Perylene Bisimide Dimer Aggregates: Fundamental Insights into Self-Assembly by NMR and UV/Vis Spectroscopy. *Chem. Eur. J.* **2012**, *18*, 13665-13677.

(40) Korevaar, P. A.; Schaefer, C.; de Greef, T. F. A.; Meijer, E. W. Controlling Chemical Self-Assembly by Solvent-Dependent Dynamics *J. Am. Chem. Soc*. **2012**, *134*, 13482-13491.

(41) (a) Valera, J. S.; Gómez, R.; Sánchez, L. Supramolecular Polymerization of [5]Helicenes. Consequences of Self-Assembly on Configurational Stability. *Org. Lett.* **2018**, *20*, 2020-2023; (b) Chan, A. K.-W.; Wong, K. M.-C.; Yam, V. W.-W. Supramolecular Assembly of Isocyanorhodium(I) Complexes: An Interplay of Rhodium(I)···Rhodium(I) Interactions, Hydrophobic–Hydrophobic Interactions, and Host–Guest Chemistry*J. Am. Chem. Soc*. **2015**, *137*, 6920−6931.

(42) (a) Mayoral, M. J.; Rest, C.; Stepanenko, V.; Schellheimer, J.; Albuquerque, R. Q.; Fernández, G. Cooperative Supramolecular Polymerization Driven by Metallophilic Pd···Pd Interactions. *J. Am. Chem. Soc*. **2013**, *135*, 2148–2151. (b) Rest, C.; Mayoral, M. J.; Fucke, K.; Schellheimer, J.; Stepanenko, V.; Fernández, G. Self-Assembly and (Hydro)gelation Triggered by Cooperative π–π and Unconventional CH···X Hydrogen Bonding Interactions. *Angew. Chem. Int. Ed*. **2014**, *53*, 700–705. (c) Kulkarni, C.; Bejagam, K. K.; Senanayak, S. P.; Narayan, K. S.; Balasubramanian, S.; George, S. J. Dipole-Moment-Driven Cooperative Supramolecular Polymerization. *J. Am. Chem. Soc*. **2015**, *137*, 3924−3932.

(43) (a) von Krbek, L. K. S.; Schalley, C. A.; Thordarson, P. Assessing cooperativity in supramolecular systems. *Chem. Soc. Rev.* **2017**, *46*, 2622-2637. (b) Mayoral, M. J.; Bilbao, N.; González-Rodríguez, D. Hydrogen-Bonded Macrocyclic Supramolecular Systems in Solution and on Surfaces. *ChemistryOpen* **2016**, *5*, 10. (c) Aparicio, F.; Mayoral, M. J.; Montoro-García, C.; González-Rodríguez, D. Guidelines for the assembly of hydrogen-bonded macrocycles. *Chem. Commun*. **2019**, *55*, 7277. (d) Romero-Pérez, S.; Camacho-García, J.; Montoro-García, C.; López-Pérez, A. M.; Sanz, A.; Mayoral, M. J.; González-Rodríguez, D. G-Arylated Hydrogen-Bonded Cyclic Tetramer Assemblies with Remarkable Thermodynamic and Kinetic Stability. *Org. Lett.* **2015**, *17*, 2664−2667. (e) Montoro-García, C.; Camacho-García, J.; López-Pérez, A. M.; Mayoral, M. J.; Bilbao, N.; González-Rodríguez, D. Role of the Symmetry of Multipoint Hydrogen Bonding on Chelate Cooperativity in Supramolecular Macrocyclization Processes. *Angew. Chem. Int. Ed.* **2016**, *55*, 223–227.

(44) Safont-Sempere, M. M.; Fernández, G.; Würthner, F. Self-Sorting Phenomena in Complex Supramolecular Systems. *Chem. Rev.* **2011**, *111*, 5784.

(45) (a) Grimme, S. Semiempirical GGA-type density functional constructed with a long-range dispersion correction. *J. Comput. Chem*. **2006**, *27*, 1787-1799. (b) Ditchfield, R.; Hehre, W. J.; Pople, J. A. Self-Consistent Molecular-Orbital Methods. IX. An Extended Gaussian-Type Basis for Molecular-Orbital Studies of Organic Molecules. *J. Chem. Phys*. **1971**, *54*, 724-728. (c) Francl, M. M.; Pietro, W. J.; Hehre, W. J.; Binkley, J. S.; Gordon, M. S.; Defrees, D. J.; Pople, J. A. Self-consistent molecular orbital methods. XXIII. A polarization-type basis set for second-row elements. *J. Chem. Phys.* **1982**, *77*, 3654. (d) Rassolov, V. A.; Ratner, M. A.; Pople, J. A.; Redfern, P. C.; Curtiss, L. A. 6-31G* basis set for third-row atoms. *J. Comput. Chem*. **2001**, *22*, 976-984.

(46) Bannwarth, C.; Ehlert, S.; Grimme, S. GFN2-xTB—An Accurate and Broadly Parametrized Self-Consistent Tight-Binding Quantum Chemical Method with Multipole Electrostatics and Density-Dependent Dispersion Contributions. *J. Chem. Theory Comput.* **2019**, *15*, 1652–1671.

(47) Kumar, J.; Tsumatori, H.; Yuasa, J.; Kawai, T.; Nakashima, T. Self-Discriminating Termination of Chiral Supramolecular Polymerization: Tuning the Length of Nanofibers *Angew. Chem., Int. Ed.* **2015**, *54*, 5943.

(48) Henderson, W. R.; Castellano, R. K. Supramolecular polymerization of chiral molecules devoid of chiral centers *Polym. Int*., **2020**, 10.1002/pi.6111.